

RC 6663 (#28655) 8/1/77  
Physics (General) 36 pages

# Research Report

## PROFILING HYDROGEN IN MATERIALS USING ION BEAMS

J.F. Ziegler, C.P. Wu, P. Williams, C.W. White, B. Terreault, B.M.U. Scherzer, R.L. Schulte, E.J. Schneid, C.W. Magee, E. Ligeon, J. L'Ecuyer, W.A. Lanford, F.J. Kuehne, E.A. Kamykowski, W.O. Hofer, A Guivarc'h, C.H. Filleux, V.R. Deline, T. Congedo, B.L. Cohen, G.J. Clark, W.K. Chu, C. Brassard, R.S. Blewer, R. Behrisch, B.R. Appleton, and D.D. Allred

Typed by Linda P. Rubin on CMC (JZ.1068)



Research Division  
San Jose · Yorktown · Zurich

## PROFILING HYDROGEN IN MATERIALS USING ION BEAMS

J.F. Ziegler, C.P. Wu, P. Williams, C.W. White, B. Terreault, B.M.U. Scherzer, R.L. Schulte, E.J. Schneid, C.W. Magee, E. Ligeon, J. L'Ecuyer, W.A. Lanford, F.J. Kuehne, E.A. Kamykowski, W.O. Hofer, A Guivarc'h, C.H. Filleux, V.R. Deline, T. Congedo, B.L. Cohen, G.J. Clark, W.K. Chu, C. Brassard, R.S. Blewer, R. Behrisch, B.R. Appleton, and D.D. Allred

Typed by Linda P. Rubin on CMC (JZ.1068)

ABSTRACT: Over the last few years many ion beam techniques have been reported for the profiling of hydrogen in materials. We have evaluated 9 of these using similar samples of hydrogen ion-implanted into silicon. When possible the samples were analysed using two or more techniques to confirm the ion-implanted accuracy. We report the results of this analysis which has produced a consensus profile of H in silicon which is useful as a calibration standard. The analytical techniques used have capabilities ranging from very high depth resolution ( $\approx 50 \text{ \AA}$ ) and high sensitivity ( $<1 \text{ ppm}$ ) to deep probes for hydrogen which can sample throughout thin sheets (up to 0.2 mm thick).

Submitted to:

Third International Conference on Ion Beam Analysis  
June 27 - July 1, 1977  
Washington, D.C.

## LIMITED DISTRIBUTION NOTICE

This report has been submitted for publication elsewhere and has been issued as a Research Report for early dissemination of its contents. As a courtesy to the intended publisher, it should not be widely distributed until after the date of outside publication.

Copies may be requested from:  
IBM Thomas J. Watson Research Center  
Post Office Box 218  
Yorktown Heights, New York 10598

AUTHOR ADDRESSES

J.F. Ziegler  
IBM Research, Box 218, Yorktown Heights, New York 10598

P. Williams and V.R. Deline  
Materials Research Laboratory, University of Illinois, Urbana, Illinois 61801

C.W. White, G.J. Clark, D.D. Allred, and B.R. Appleton,  
Solid State Div., Oak Ridge National Lab., Oak Ridge, Tennessee 37830

B. Terreault,  
Centre de l'Energie, INRS, Universite du Quebec, C.P. 1020 Varennes, Quebec, Canada

B.M.U. Scherzer, W.O. Hofer, and R. Behrisch,  
Max-Planck-Inst. fur Plasmaphysik, D. 8046 Garching, West Germany

R.L. Schulte, E.J. Schneid, F.J. Kuehne, and E.A. Kamykowski,  
Research Department, Grumman Aerospace Co., Bethpage, New York 11714

C.W. Magee and C.P. Wu  
RCA Laboratories, Princeton, New Jersey 08540

E. Ligeon  
Centre d'Etudes Nuclaires de Grenoble, Section de Physique Du Solides,  
BP-85, Centre de tri 38041, Grenoble, France

A. Guivarc'h  
Centre National des Telecommunications, PMT, 22301, Lannion, France

C.H. Filleux  
Kellogg Rad. Lab., California Institute of Technology, Pasadena, California 91125

J. L'Ecuyer and C. Brassard,  
Laboratoire de Physique Nucleaire, Universite de Montreal, C.P. 6128, Montreal, Canada

C.A. Evans, Jr.  
School of Chemical Sciences, University of Illinois, Urbana, Illinois 61801

W.A. Lanford,  
Nuclear Structure Lab., Physics Dept., Yale University, New Haven, Conn. 06520

B.L. Cohen and T. Congedo,  
Physics Dept., University of Pittsburgh, Pittsburgh, Penna. 15213

W.K. Chu,  
IBM-SP Division, East Fishkill, Hopewell Junction, N.Y. 12533

R.S. Blewer  
Applied Physics, Div. - 2353, P.O. Box 5800, Albuquerque, N.M. 87115

## PROFILING HYDROGEN IN MATERIALS USING ION BEAMS

Over the last few years many ion beam techniques have been evaluated for profiling hydrogen in materials. These techniques have proven useful in such applications as solar wind effects on moon rocks; dating of glass artifacts; fusion reactor first-wall studies; studies on amorphous silicon solar cells; and hydrogen embrittlement of steels and niobium. In general the techniques are non-destructive, have a depth resolution of about 20 nm, and require about 60 minutes running time for each sample.

There are eight basic approaches to hydrogen profiling with ion beams, with 14 variations. These are summarized in Table 1 and References 1-14. Each will be described in detail below.

We report a round-robin comparative study of 9 of these techniques using identical samples of hydrogen implanted into silicon. Since several of the other ion beam techniques were not applicable to the target chosen for the round-robin, we include brief descriptions of these for completeness with mention of their particular advantages.

### SAMPLE PREPARATION

Silicon was chosen as the host material for this study for several reasons: (a) it has extremely high purity with no known hydrogen incorporated into the bulk material, (b) it can be obtained with highly polished surfaces, (c) it is believed to trap ion-implanted hydrogen with high efficiency, and (d) silicon is a technologically important material. The hydrogen was ion-implanted into the silicon to provide reproducible hydrogen concentrations with sharp concentration gradients. These gradients provide a test of the depth resolution of the various techniques.

The samples were made from Si <100> single crystals, 2.54 cm in diameter, with a surface chemically polished to better than 1 nm.<sup>15</sup> These wafers were etched in buffered HF, and then ion-implanted with Si at 270 keV,  $1 \times 10^{15}$  Si/cm<sup>2</sup>, to make the surface amorphous

and to provide traps for the implanted hydrogen. The wafers were then implanted with hydrogen to doses of  $10^{16}$  H/cm<sup>2</sup> using an electrostatically rastered beam which swept each wafer more than  $10^3$  times to obtain high implantation uniformity. (Several wafers were implanted with higher doses, and these will be identified later.) The wafers were Ga backed to a heat-sink during ion implantation to prevent annealing of the amorphous Si layer. Some of the wafers were implanted with protons, <sup>1</sup>H, at 40 keV ( $\pm 2$  keV), and others were implanted with deuterons, <sup>2</sup>H, at 31 keV ( $\pm 2$  keV). Calculations<sup>16</sup> indicated that these energies would provide for a hydrogen peak at 400 nm, although the proton implantation distribution would be narrower than the deuterium distribution. The proton width was calculated to be 100 nm (FWHM) while the deuterium width would be 140 nm.

A sample was then sent to each of the laboratories concerned, it was analysed, and then it was sent on to a second laboratory to confirm the accuracy of the original implantation.

## GENERAL RESULTS

The general results are shown in Figure 1. Each laboratory reported a hydrogen concentration profile which was reduced to three hydrogen profile characteristics: Range, Straggling (FWHM), and Total Dose. The hydrogen range was defined as the depth of the hydrogen peak. The straggling was the hydrogen peak width measured at full-width at half-maximum (FWHM). The total dose was defined as the total hydrogen content found in the sample, using units of H/cm<sup>2</sup>.

The upper portion of Figure 1 shows the ranges determined by each laboratory. The numbers in parenthesis indicates that this measurement was a second independent evaluation of the same sample. As can be seen there is remarkably good agreement, with a standard error of 8% (i.e., 68% of the samples were within this much of the mean). It is believed that this error is mostly due to inaccurately known stopping powers for the various ions. A second possible source of error is the identification of the target surface, but normal contamination of

sample surfaces by water vapor and adsorbed hydrocarbon layers makes identification of the surface for  $^1\text{H}$  profiling rather simple. For  $^2\text{H}$  profiling, a surface monolayer can be achieved on some samples by evaporating deuterated liquids on the surface.

The middle portion of Figure 1 shows that the H concentration peak widths as determined by the various techniques. The analysis of the proton and deuteron distributions are quite consistent, with a standard error about the same as for the range measurements.

The lower portion of Figure 1 shows the total H concentration found in each sample. The original ion-implanted proton doses were nominally  $10^{16}$  H/cm<sup>2</sup>, but calculations and experiments<sup>17</sup> have shown that about .9% of the H would be reflected from the Si samples, so the actual proton implanted dose was  $9.9 \times 10^{15}$  H/cm<sup>2</sup>. The deuterium implantation dose was 10× higher than the proton dose.

We conclude that with proper concern for using accurate cross sections and stopping powers, and with proper identification of the sample surface, hydrogen can be profiled in Si with an absolute accuracy better than 8% up to depths of about 600 nm.

## COMMENTS ON SPECIFIC TECHNIQUES

The typical experimental conditions for the analysis of H in Si are summarized in Table 2. Two items are of special comparative interest and are listed at the bottom of the Table. One line tabulates the energy put into the sample which is converted into heat (watts). Since hydrogen is highly mobile in most materials (typical diffusivity in metals is  $10^{-6}$  cm<sup>2</sup>/sec at room temperature) the use of beams which minimize target heating is an advantage if a wide variety of materials are to be analysed. The last line in Table 2 is an estimated depth resolution (FWHM) for each technique for profiling H in Si at a depth of  $\sim 400$  nm.

It should be emphasized that these quantities are only applicable to Si, and each technique will have different parameters for other target materials.

## EXPERIMENTAL DETAILS

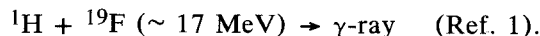


Figure 3 is a drawing of one type of experimental set up for hydrogen profiling using a nuclear reaction which produces a  $\gamma$ -ray (this arrangement is described in detail in Ref. 1e).

Two aspects are noteworthy:

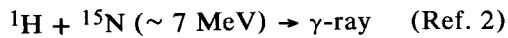
1. Two NaI(Tl) crystals were used to detect  $\gamma$ -rays, with typical spectra shown in Fig. 4. After the spectra were corrected for background the yields from each detector were summed.
2. The total charge collected was determined by two methods:
  - a. The charge was integrated from the target holder which was surrounded by a suppressor biased at -300 V for secondary electron suppression.
  - b. The beam was sampled by a rotating flipper which scattered particles from the beam into a surface barrier detector. This was calibrated

using a Faraday cup. Consistent results were obtained for both techniques.

To obtain the depth and absolute hydrogen concentration from the  $\gamma$ -ray yield two quantities, the ion stopping power and a H concentration calibration constant, had to be determined. The stopping powers used for  $^{19}\text{F}$  were obtained by interpolating the values given by Northcliffe and Schilling.<sup>18</sup> These values were independently checked on a thin hydrogenated amorphous silicon film<sup>1e</sup> using the backscattering of 1 and 2 MeV  $\alpha$  particles and the Talysurf technique.<sup>19</sup> The thickness determined by Talysurf was 16% smaller than the  $^4\text{He}$  backscattering results. The  $^{19}\text{F}$  data gave a depth 9% smaller than the backscattering.

The hydrogen content of the ion implanted samples studied was determined in absolute terms by comparing  $\gamma$ -ray yields with similar yields obtained (1) from materials containing hydrogen and having a well-established stoichiometry namely Lexan  $[(\text{C}_{16}\text{H}_{14}\text{O}_3)_n]$  and polyethylene  $[(\text{CH}_2)_n]$  and (2) from a silicon wafer implanted with a known H dose. Using this approach the problems associated with using absolute cross sections are avoided. Likewise any anisotropies in the  $\gamma$ -rays emitted can be ignored.

In general obtaining the correct hydrogen profile is complicated by off-resonance contributions to the  $\gamma$ -ray yield as indicated in Figure 5. Corrections for the off-resonance yield must be made to the  $^{19}\text{F}$  profile data when the 16.44 MeV resonance is used. In fact, using the  $^{19}\text{F}$  beam rather accurate estimations of the average hydrogen content in the bulk of a sample (e.g.  $1\mu$  to  $4\mu$  in  $\text{SiO}_2$ ) can be obtained from the yield data taken below resonance.<sup>1e</sup> Yield profiles can be unfolded using the cross section data of Maurel et al.<sup>20</sup>



The  ${}^{15}\text{N}$  hydrogen profiling method makes use of a narrow, isolated resonance to measure the hydrogen concentration vs. depth in solids. If the sample is bombarded with  ${}^{15}\text{N}$  at the resonance energy (6.385 MeV), the yield of 4.43 MeV gamma-rays is proportional to the hydrogen concentration on the surface. If the beam energy is raised, the hydrogen on the surface will not be detected because the cross-section above the resonance is three orders of magnitude smaller than the resonance cross-section. As the  ${}^{15}\text{N}$  slows down passing through the solid, it reaches the resonance energy at some depth. The resonant  $\gamma$ -ray yield is proportional to the hydrogen concentration at that depth. Hence, to determine the hydrogen concentration vs. depth, the yield of characteristic  $\gamma$ -rays is measured vs  ${}^{15}\text{N}$  energy.

The  ${}^{15}\text{N}$  beam is incident on the target as shown in Fig. 6 and the yield of gamma-rays is measured with a 3 inch by 3 inch NaI detector outside the vacuum detector about 1 inch behind the target. For convenience the targets are mounted on a wheel so that they can be changed remotely.

Shown in Figure 7 are two spectra measured with the NaI detector. Both were accumulated for 6 hours, one with beam on and one with beam off. The difference between the two spectra is the 4.43 MeV gamma-ray peak and its associated escape peaks and Compton edge.

The raw data for the hydrogen profile measured for the present example,  $10^{16}$  H/cm<sup>2</sup> at 40 keV implanted into silicon, is shown in Fig. 8. The bottom and left axis are the beam energy and gamma-ray yield. The beam intensity was about 50 namps (particle current), hence a 5  $\mu$  coulomb data point took about 100 sec. Because the characteristic  $\gamma$ -ray from this reaction is a high energy gamma-ray, the background in this energy region is small. The counts plotted in Fig. 8 are simply the counts observed in a single channel analyzer window set to count from 3.3 to 4.8 Me (see Fig. 7). The ambient background in this region without any shielding is about 4 counts/min.

In order to convert this  $\gamma$ -ray yield (Fig. 8) to a plot of hydrogen concentration vs. depth, it is necessary to know (1) the product of the cross-section for the resonance reaction and detector efficiency and (2) the rate of energy loss of 6.5 - 7.0 MeV  $^{15}\text{N}$  in the target material. In order to determine (1), we profiled two calibration samples made of sapphire implanted with accurately known doses of hydrogen. By integrating the profiles and equating these with the known doses, the calibration is obtained. It should be pointed out that this procedure is independent of the  $dE/dx$  assumed for  $^{15}\text{N}$  in sapphire.

We used four different methods to obtain  $dE/dx$  for  $^{15}\text{N}$  in silicon: Northcliffe and Schilling,<sup>18</sup> corrected using Ziegler and Chu  $^4\text{He}$  stopping powers<sup>21</sup> for  $Z_2$  oscillations,<sup>25,26</sup> theories of Lindhard and Winther,<sup>22</sup> and Nesbet and Ziegler.<sup>23</sup> The results were, respectively: 1.55, 1.50, 1.49 and 1.44 MeV/ $\mu\text{m}$ . We used the average, 1.50 MeV/ $\mu\text{m}$ . Once  $dE/dx$  has been determined, the yield of  $\gamma$ -ray vs. energy is converted to hydrogen concentration vs. depth using (depth into solid) =  $(E - E_{\text{RES}})/(dE/dx)$  where  $E_{\text{RES}}$  is the resonance energy. The concentration scale is given by (hydrogen concentration) = (constant)  $(dE/dx)$  ( $\gamma$ -ray yield/ $\mu$  Coul.) where the constant is dependent only on the product of the resonant cross-section and detector efficiency and was determined by the calibration procedure outlined above. These scales are shown on the top and right in Fig. 8.

There are some general comments which should be made concerning this method. First, for any target this reaction can give a signal only from H. The  $^{15}\text{N}$  is below the Coulomb barrier for reactions with all elements other than H and, consequently, cannot undergo nuclear reactions with any other element. Second, the depth resolution near the surface is narrower than previously published. In the present case it is about 4 nm. Analysis of surface peaks, such as that shown in Fig. 8, shows that the literature value for the width of this resonance is not 0.9 keV (C.M.) but more like 0.4 keV. This improved depth resolution has at least one important consequence. Namely, the everpresent hydrogen surface peak does not extend into depths for more than a few hundred Angstroms. This allows one to probe the near surface

region. This is in contrast to a reaction such as that induced with  $^{19}\text{F}$ . Third, there is a larger cross-section resonance at 13.351 MeV ( $^{15}\text{N}$  lab.) which could be used if additional count rate is desirable. This resonance has a gamma-ray yield/ $\mu$  coul. about ten times greater than the 6.385 MeV resonance. This greater sensitivity is achieved with a loss of depth resolution; the higher energy resonance has a depth resolution of about 215 Å at the surface.



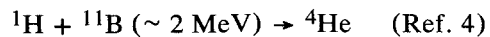
This method for measuring hydrogen concentrations profiles within the near surface region of material makes use of the  $^1\text{H}(^7\text{Li}, \gamma)^8\text{Be}$  reaction. At the resonance energy of 3.07 MeV the emitted 17.6 MeV gamma rays of  $^8\text{Be}$  are detected by a 20 cm  $\times$  15 cm NaI detector with a plastic anti-coincidence scintillator and the spectrum is accumulated and stored by an on-line computer system. A typical pulse height spectrum (Figure 9) shows the 17.6 MeV gamma ray group and a 14.7 MeV group resulting from the decay to a broad state in  $^8\text{Be}$  at 2.90 MeV. The 17.6 and 14.7 MeV gamma ray yields are proportional to the hydrogen concentration within the reaction volume of the specimen under study. The cosmic ray background is very efficiently reduced through the use of the plastic anti-coincidence scintillator. The count rate due to cosmic rays is typically 0.01 cts/sec.

In order to determine the absolute hydrogen concentration a comparison is made between the  $\gamma$ -ray yield of the sample and that of a reference sample whose hydrogen content is known. A correction is applied to account for the differences in stopping power in the reference and sample specimens. National Bureau of Standards hydrogen-in-titanium standards are used as reference samples. The as-received surfaces are removed by mechanical means to expose the interior of the sample. In order to be acceptable, each standard used is required to have a uniform distribution of hydrogen over a 2  $\mu\text{m}$  probing depth, and for the calibration to be valid,  $\gamma$ -ray yields from each must be in proportion to the known bulk hydrogen concentration

(0.16, 0.5 and 1.0 atomic percent hydrogen). Details of this calibration procedure can be obtained from the authors of Ref. 3 a,b,c.

Figure 10 shows the concentration profile for a hydrogen implanted silicon sample. Results are shown for two separate measurements (taken a week apart) that were individually calibrated with different sets of hydrogen-in-titanium reference standards. The peak at 3.07 MeV corresponds to a high hydrogen concentration at the surface of the sample. The centroid of the 40 keV H implantation peak is located at 0.44  $\mu\text{m}$ . The depth scale is derived from the stopping power compilation of Northcliffe and Schilling.<sup>18</sup> The resonance width of the reaction, a depth resolution of 170 nm, has not been extracted from the profile. However, on deconvoluting the resonance width from these data, we obtain the range straggling of 105 nm for the 40 keV hydrogen implant.

The  ${}^1\text{H}({}^7\text{Li}, \gamma) {}^8\text{Be}$  reaction is capable of measuring hydrogen concentrations to a depth of 8  $\mu\text{m}$  with a level of detectability of slightly less than 0.1 atomic percent in most metals.



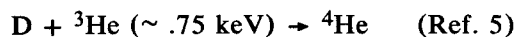
The schematic drawing of the experimental apparatus is represented on Fig. 11. The incident  ${}^{11}\text{B}$  beam ( $\sim 2 \text{ MeV}$ ) interacts with hydrogen in the sample with the nuclear reaction  ${}^{11}\text{B} + {}^1\text{H} \rightarrow \alpha + {}^8\text{Be} \rightarrow \alpha + 2 \alpha$ . This reaction is isotropic<sup>24</sup> with a cross-section estimated to be  $\approx 8 \text{ mb/str}$  at resonance. The product  $\alpha$ -particles are detected by a surface barrier detector covered by a 3  $\mu\text{m}$  mylar absorber to eliminate scattered  ${}^{11}\text{B}$  ions (see fig. 11). The experimental excitation data of the proton implanted silicon sample is shown on fig. 12 (this data is the average of three different runs).

On another silicon sample we have measured the energy loss of the incoming boron beam and found  $dE/dx \sim 810 \text{ keV}/\mu\text{m}$ . This value is slightly lower than our previous measurement<sup>4b</sup> of  $880 \text{ keV}/\mu\text{m}$ .

The excitation data plotted after some layers have been removed with anodic oxidation (0, 1000 Å, 1500 Å, 2000 Å, 2500 Å) are shown in Fig. 13. The value of  $dE/dx = 810 \text{ keV}/\mu\text{m}$  is used to transform the energy scale into a depth scale (see fig. 12).

To extract the hydrogen profile from the excitation data (fig. 12) we have used a convolution process. We assume that hydrogen profile is made up of a thin layer of surface contamination and by a hydrogen distribution at the implantation depth  $R_p$ . At first we assumed a Gaussian distribution defined by  $R_p$  and a standard deviation  $\sigma_t$ . The fit of the excitation curve (shown as a solid line in fig. 12) was calculated assuming a Gaussian distribution corresponding to  $R_p \sim 6100 \text{ Å}$  and  $\sigma_H \sim 620 \text{ Å}$  (sample tilted at  $45^\circ$  from the incident beam direction) and the resulting calculated spectrum is shown in fig. 14. We obtain good agreement between the experimental and the computed excitation curve. A fit of the excitation curve performed from a dissymmetrical hydrogen distribution appears unnecessary. It must be pointed out that the width of the excitation curve (in fig. 12) takes into consideration several standard deviations since  $\sigma_t^2 \approx \sigma_H^2 + \sigma_R^2 + \sigma_s^2$ .

- $\sigma_t$  = total standard deviation deduced by fitting of the experimental excitation curve.
- $\sigma_H$  corresponds to the standard deviation of the implanted hydrogen profile.
- $\sigma_R$  is the standard deviation corresponding to the resonance width of the nuclear reaction  $\Gamma_R \approx 66 \text{ keV} \rightarrow \sigma_R \sim 350 \text{ Å}$ .
- $\sigma_s$  is the standard deviation due to the straggling of the  $^{11}\text{B}$  analyzing beam.  $\sigma_s$  has not been found important in this experiment. This is clear in fig. 13 where the widths of the excitation curves are independent of the layer thickness taken off by anodic oxidation.



The application of the  $\text{D} + {}^3\text{He} \rightarrow \alpha + \text{p}$  nuclear reaction with a Q value of 18.35 MeV

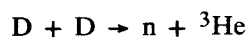
for profiling deuterons in solids is shown schematically in fig. 15. The cross-section is isotropic and for incident energies of 750 keV a constant cross section of  $70 \text{ mb} \pm 5\%$  can be assumed for depths up to 500 nm [ref. 5e and 5f]. The depth profile is obtained from the energy distribution of the outgoing  $\alpha$ -particles and no window can be used in front of the high resolution surface barrier detector. There are 2 to 3 orders of magnitude more backscattered  $^3\text{He}$  ions (depending on the substrate material), and the count rate for  $^4\text{He}$  is low (about 1 per sec). It could, however, be improved by electromagnetically separating the lower energy  $^3\text{He}$  ions from the higher energy  $^4\text{He}$  ions.

In order to determine the surface location in the  $\alpha$ -spectrum the detector must be energy calibrated. This was performed with an  $^{241}\text{Am}$ -spectrum and backscattering spectra at several incident ion energies. Also, the experimental geometry must be known to better than  $1^\circ$  for calculating the energy of  $\alpha$ -particles produced at the target (typically 3 to 4 MeV). The protons produced in the reaction have an energy of about 15 MeV. As they lose only part of their energy within the depletion layer of the detector, they can be found at different energies in the spectrum, depending on the bias voltage of the detector (fig. 15).

The absolute amount of implanted D can be obtained from the integrated proton peak or the  $\alpha$ -peak if the  $^3\text{He}$  dose and the angle of the detector are known. These two quantities enter also into the height of the  $^3\text{He}$  backscattering spectrum if channeling is avoided. Thus the ratio between the integrated  $^4\text{He}$  (or proton) counts and the height of the backscattering spectrum give directly the total amount of implanted D [ref. 5f].

In order to obtain the depth profile from the  $^4\text{He}$  spectrum, the stopping powers of  $^3\text{He}$  and  $^4\text{He}$  have to be known. In this work, the values of Ziegler and Chu<sup>21</sup> have been used. For getting good depth resolution, flat surfaces and large angles  $\beta$  have to be used.<sup>5d</sup> Then a near-surface resolution of  $\sim 3 \text{ nm}$  can be obtained. For larger depths the resolution gets wider due to fluctuations in the stopping power and the finite acceptance angle of the detector.

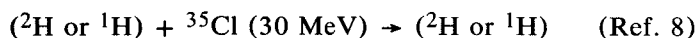
The technique described is applicable for all solids. It has already successfully been used for D profiling in C, Ti, Zr, Si and Stainless Steel.<sup>5c,f,g</sup>



See Ref. 6.



See Ref. 7, and paper by J.C. Davis, H.W. Lefevre, and C.H. Poppe in this issue.



The technique  $\text{H} + {}^{35}\text{Cl} \rightarrow \text{H} + {}^{35}\text{Cl}$  is essentially similar to Nuclear Backscattering spectrometry. The main difference, of course, is that we are detecting the recoiling nucleus (here H) rather than the scattered incident particle. The layout that is used is indicated in figure 16.

Since we are looking at recoils, the detector angle  $\theta$  must be small. This means that with thick targets, the normal to the surface must make a large angle with the beam direction therefore requiring an accurate goniometer and reducing the thickness that can be explored (here 1  $\mu\text{m}$ ). A filter (normally mylar) just thick enough to stop the high flux of elastically scattered  ${}^{35}\text{Cl}$  ions must be used to prevent them from reaching the detector. The energy of the  ${}^{35}\text{Cl}$  beam (30 MeV) is chosen so as to maximize its stopping power,  $dE/dx$ , while at the same time being much below the Coulomb barrier to eliminate nuclear reactions from any element. The kinematic energy variation with angle being large, narrow slits must be used in front of the detector.

A typical spectrum is shown in figure 17. It is similar to a standard backscattering spectrum and its analysis has been done by the same techniques. The  $dE/dx$  have been taken

from the tables of Northcliffe and Schilling<sup>18</sup> and the scattering cross sections have been computed from the Rutherford formula.

The main advantage of this method is its generality. It can be used to profile simultaneously all elements lighter than  $^{20}\text{Ne}$ , with similar depth resolution ( $\sim 10$  nm) and sensitivity ( $< 10^{15}$  H/cm<sup>2</sup>). Thin targets can be analyzed by transmission, thereby lifting the requirement of large target tilt. No evidence of sputtering of the target by the  $^{35}\text{Cl}$  beam was observed after repeated runs.



NOTE: The following technique was inappropriate for the round-robin sample, and is not shown in Fig. 1.

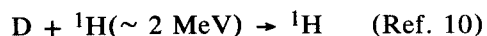
In the transmission-coincidence method (Fig. 18), two equal energy protons (or deuterons) are detected in fast coincidence and the sum of their energies is recorded. The energy loss is larger after the scattering event than before because: (1) there are two protons losing energy rather than just one, (2) their path length through the material is increased by a factor of 1.4 because their directions are at  $45^\circ$  to the normal, and (3) each particle has half the initial energy which means roughly twice the rate of energy loss. Thus the energy loss per micron of thickness is about  $2 \times 1.4 \times 2 \approx 5.6$  times larger after the scattering than before, and the summed energy is therefore larger if the hydrogen is located near the front of the foil (beam entering side) than if it is near the back.

A typical measurement of the summed energy distribution is shown in Fig. 19. The two peaks are due to hydrogen on the surfaces. It is usually sufficiently accurate to assume a linear relationship between summed energy and depth, with these peaks marking zero and full depth, so the depth profile is just the summed energy with this calibration. Corrections to intensity

are needed to correct for multiple scattering, and if samples are especially thick, small corrections should be applied for non-linearity in the depth versus summed energy relationship.

This method has also been used for helium analysis and can easily be used for deuterium analysis. In the latter, thin deuterated films can be placed on the two surfaces in a calibration run, and in the former special foils with helium impregnation were prepared for the calibration. In normal hydrogen analysis, intensity calibration is done with thin plastic films of known hydrogen content placed over each surface; this also determines the multiple scattering correction.

Since this technique is absolutely specific for the nucleus under study, problems of background subtraction are eliminated, which enhances sensitivity. Measurements have been made of hydrogen contents below 0.1 ppm by weight. All calibrations are contained in the experiment with no need for cross sections or stopping powers. Data analysis is trivial, with no need for deconvolutions. The incident beam energy can be adjusted to fit the sample thickness (if sufficient beam energy is available); best results are obtained if about 10% of the beam energy is lost in traversing the sample. The depth resolution is 5-10% of the sample thickness.



The direct backscattering technique can be used to detect and profile very low-Z impurity distributions in higher Z substrates, a fact which was generally unrecognized until recently.<sup>27</sup> The method can be used both on thick and thin target substrates for all impurities whose mass is greater than one atomic mass unit. Detection sensitivity is greater on foil targets than on thick targets because background problems largely disappear. However, good results are also achievable using thick targets; a thick silicon wafer was used in this study to demonstrate this point and also to provide internal consistency with other experiments reported in this paper.

The technique consists of bombarding a deuterium implanted silicon sample with a monoenergetic collimated beam of protons at an energy of 2.0 - 2.5 MeV and then energy analyzing those protons elastically scattered at a high angle with respect to the incident beam direction (typically  $160^\circ$  -  $170^\circ$ ). A schematic representation of the experimental arrangement and a typical spectrum is shown in Figure 20. Energy analysis is most often accomplished using a standard surface barrier detector, though electrostatic<sup>28</sup> or magnetic<sup>29</sup> energy analysis has also been used for very high resolution work. Protons backscattered from each of the elements comprising the surface of the target arrive at the detector with a unique energy  $E_1$ , which is determined by the mass of the struck target atom  $M_2$  the initial energy  $E_0$ , of the incident protons of mass  $M_1$ , and the laboratory scattering angle  $\theta$ , according to the relation

$$E_1 = k E_0 \text{ where } k = \left[ \frac{\cos \theta + [(M_2/M_1)^2 - \sin^2 \theta]^{1/2}}{1 + M_2/M_1} \right]^2 \quad (1)$$

This study involves profiling a deuterium distribution implanted in silicon at 31 keV. A raw data plot of backscattered proton counts versus backscattered proton energy is shown in Figure 21. The scattering angle of the detector was  $\theta = 164^\circ$  so that from Eq. (1),  $k_{Si} = 0.868$  and  $k_D = 0.115$ .  $E_{Si}$  and  $E_D$  for surface silicon and surface deuterium are indicated by vertical lines. The energy position of surface carbon and surface oxygen and other low-Z elements are also indicated. (The large peak at  $\sim 1.2$  MeV is not due to an impurity but to a resonance in the scattering cross section for protons on silicon.) The depth of the deuterium distribution into the Si surface is indicated by the inset depth scale which was determined from the relation

$$t = \frac{\Delta E}{N[\epsilon]} \quad (2)$$

where  $t$  is the depth at which an incident proton is backscattered,  $\Delta E = kE_0 - E_1$ ,  $N$  is the atom density and  $[\epsilon]$  is the backscattering energy loss factor defined by Eq. (3) below:

$$[\epsilon] = \frac{k_D[\epsilon_{in}]}{|\cos \theta_{in}|} + \frac{[\epsilon_{out}]}{|\cos \theta_{out}|} \quad (3)$$

For  $\Delta E \ll E_0$ , the relationship between  $t$  and  $\Delta E$  is linear and a depth scale for each element present in the sample can easily be determined. The energy at which protons scattered from deuterium on the surface of the sample is determined explicitly from Eq. (1), so there is no ambiguity about specifying the zero position of the depth scale for any impurity elements present. Stopping cross sections as a function of energy are tabulated in several publications. Those used for this data reduction are from Ref. 16.

The concentration of the implanted deuterium can be determined from a knowledge of the elastic scattering cross section of deuterium (hydrogen) for 2.5 MeV protons. The data of Kocher and Clegg<sup>30</sup> were used here. The appropriate formula for the atomic areal density is given below.

$$(Nt)_D = \frac{A_D}{H_{Si}} \frac{\sigma_{Si}}{\sigma_D} \frac{\delta E_1}{[\epsilon]} \quad (4)$$

$A_D$  is the integrated number of counts from protons backscattered from deuterium,  $H_{Si}$  is the height (counts per channel) of the silicon spectrum in the near surface region,  $\delta E_1$  is the energy span per channel, and sigma is the respective differential elastic scattering cross section for protons on silicon and deuterium.

In this experiment a 25 mm<sup>2</sup>, 100  $\mu$ m depletion depth premium quality silicon detector was used with the recommended 75 V bias. No detector filter is necessary (or desirable). The detector resolution in the experiment was 8.7 keV which corresponds to a depth resolution of 8 nm for an angle of incidence of 80° from the normal and 98 nm for normal incidence. Using an electrostatic energy analyzer and grazing incidence geometry, depth resolutions below 1 nm have been demonstrated using the elastic scattering technique.<sup>28</sup> No deconvolution of the data is necessary to obtain an accurate impurity depth profile using the nuclear elastic back-scattering technique. The detector resolution does not affect the measured mean range since both the detector function and the measured profile are symmetric distributions. The detector energy spread adds ~2% to the true FWHM at 80° from the normal and 11% for normal

incidence. This correction can be made in a straight forward manner in either case.

Determination of the projected range for 31 keV deuterium in silicon agree well with theoretical calculations. The measured FWHM when corrected for detector resolution effects exceed the calculated values. This is not unexpected because the sample analyzed was implanted to higher fluences ( $5 \times 10^{17} \text{D/cm}^2$ ) than other samples and some saturational broadening is probable. The results for three trials are summarized below:

Trial 1:	$R_p = 4090 \text{Å}$	$\text{FWHM} = 1800 \text{Å} \theta = 164^\circ$
Trial 2:	$R_p = 4060 \text{Å}$	$\text{FWHM} = 2070 \text{Å} \theta = 164^\circ$
Trial 3:	$R_p = 4040 \text{Å}$	$\text{FWHM} = 1930 \text{Å} \theta = 120^\circ$
Average:	$R_p = 4060 \text{Å}$	$\text{FWHM} = 1935 \text{Å}$

It should be noted that the key factor which permits use of the conventional elastic backscattering technique in the profiling of light elements in higher Z substrates is the large enhancement in the nuclear elastic scattering cross section as the energy of the incident beam particles approaches the Coulomb barrier energy of the light impurity atoms in the target. At incident proton energies in the range of 2.0 - 2.5 MeV, the elastic cross section enhancement (over Rutherford values) ranges from a factor of  $\sim 8 - 14$  for protons on oxygen or carbon to a factor of  $\sim 200 - 400$  for protons on helium or deuterium.<sup>31</sup> This is the key to the success of this method. Because Coulombic cross sections decrease as the square of decreasing atomic charge, the possibility of observing very low Z elements in higher Z substrates is still not universally recognized as being within the capability of conventional ion backscattering.

Special attributes of this technique include the following:

1. All other low-Z impurities in the sample are profiled simultaneously. This is indispensable in sequential-event studies to monitor the surface cleanliness, oxide or carbon layer buildup, impurity migration, and release, etc.
2. The substrate is also simultaneously identified as to elemental composition, stoichiometry and (in the case of films or foils) areal density. The latter is essential information in studies in which the sample surfaces may experience

(ion) erosion, spallation and flaking or in layer-structures where interfacial diffusion may occur.

3. Proton backscattering spectra are very quickly acquired and are very simple to interpret because the technique involves purely elastic scattering. Spectra do not require deconvolution. Direct proton backscattering is capable of probing depths down to tens of micrometers and is not restricted to transmission (foil) samples. The surface position of each low-Z impurity is established kinetically. Polished samples are not required, nor are high energy, heavy ion beam accelerators or cyclotrons.
4. Limitations include the inability to detect  $^1\text{H}$  ( $^2\text{H}$  must be used instead) and lower detection sensitivity than some nuclear reaction techniques.

#### Secondary Ion Mass Spectrometry (SIMS) (Ref. 14)

In-depth concentration profiling by secondary ion mass spectrometry is achieved by sputtering the sample and simultaneously recording the intensity of the secondary ion of interest. The ion optical design of a typical instrument is described in Ref. 14a. Depth profiling techniques are described in references 14b and 14c. Other applications of the technique to studies of hydrogen embrittlement, environmental problems, and ion implant depth profiling are described in references 14d -- 14f.

Accurate depth profiling in SIMS requires careful attention to the problem of discriminating against ions sputtered from the sides of the sputtered crater. Such discrimination is necessary to ensure that the ions come from the same depth in the sample, so that the sputtering time scale can be accurately converted to a depth scale. Elimination of the crater-rim signal can be accomplished by means of either an ion-optical or an electronic aperture. The latter technique allows data accumulation only during the time that the primary ion beam spends in the central portion of the eroded area. Optimum performance is achieved by

combining both aperturing techniques. The primary ion beam is raster-scanned in order to erode a flat-bottomed crater.

A critical step in the evaluation of the raw data is to establish the depth scale. The problem of absolute concentration determination would, in principle, require knowledge of the ionization probability of the particular ion and of the transmission characteristics of the mass spectrometer. However, this problem can be overcome by using standards. Depth scales can be established either (a) from knowledge of sputtering rates or (b) by measurement of the sputtered crater depth after analysis. In multilayer samples, where sputtering rates may vary as different layers are traversed, depth scales are best established by means of a non-sputtering technique such as Rutherford backscattering spectrometry (see ref. 14g).

(a) Use of sputtering rate information.

The transformation from time to depth scale using sputtering rates requires exact knowledge of the sputtering yield and of the flux density of the primary ions. These two quantities are in general not too well known. Even in the favorable case of a Si matrix where there is no surface roughening, this uncertainty is estimated to be about 30%.

For the present deuterium profiles in amorphous Si, the erosion was performed with an 11 keV Ar<sup>+</sup> beam, raster-scanned over an area of 85 × 85 μm. The frame speed was 5.7 sec per full sweep, resulting in an erosion of 4.8 monolayers at a (focused) current of 9.5 nA and a sputtering yield of 1.5 atoms/ion. The data were obtained as described in ref. 14b. Typical results are shown in Table 3.

A special problem was met in profiling hydrogen. Here, a much higher background at mass 1 -- as compared to the background at mass 2 for deuterium -- rendered it impossible to measure the total implantation profile; only the maximum of the range distribution was significantly above this background. This effect might be due to both H redeposition from the residual gas, and the influence of the "neutral beam", i.e., a beam not influenced by the scan

generator and thus rendering electronic gating ineffective. Several methods are currently being tried to overcome this problem.

(b) Measurement of crater depths.

For the highest accuracy, the sputtering rate should be determined in situ by measuring the depth of the crater eroded during the analysis. This is necessary in any event when the sputtering yield has not been independently determined -- i.e., for non-normal incidence Ar<sup>+</sup> or for Cs<sup>+</sup> primary species. Both Talysurf and interference microscope techniques have been used to obtain the results shown in Table 3. The Talysurf was calibrated with a standard roughness sample, and the quoted errors reflect the calibration accuracy. The errors quoted for Cs<sup>+</sup> are the standard deviation of the interference microscope measurements. No attempt has been made to estimate systematic errors in this case.

Hydrogen and deuterium profiles obtained using Ar<sup>+</sup> and Cs<sup>+</sup> bombardment SIMS respectively are shown in Figures 22 and 23. The hydrogen profile obtained in the Cs<sup>+</sup> instrument exhibits a high background (about 20% of the peak implant signal) due to residual hydrogen-bearing species in the sample chamber (background pressure  $1.5 \times 10^{-8}$  Torr). These species can adsorb onto the freshly eroded surface giving rise to a signal which at the pressure quoted is equivalent to that produced by a sample concentration of about  $4 \times 10^{19}$  atom/cm<sup>3</sup>. The H profile shown in Figure 22 was obtained in an instrument with a UHV sample chamber. Hydrogen secondary ion background in this instrument is further reduced through elimination of the neutral beam emanating from the primary ion source, and through the use of stigmatic imaging secondary ion optics to combine ion optical aperturing with the electronic aperturing technique.

### Quantitation

To convert secondary ion intensity ratios to concentration values, comparison with standard samples is required. No well-characterized bulk samples were available to us.

Comparison was made with other ion-implanted samples (H implanted into Si single-crystal substrates). The round-robin doses were found to be:

$$\text{H } 1.3 \times 10^{16} \text{ atom/cm}^2 \text{ (Cs}^+\text{)}$$

$$\text{H } 6.0 \times 10^{15} \text{ atom/cm}^2 \text{ (Ar}^+\text{)}$$

$$\text{D } 9.0 \times 10^{16} \text{ atom/cm}^2 \text{ (Cs}^+\text{)}$$

The deuterium dose was calculated by reference to a proton implant standard. The calculation involves the assumption that the yield of H<sup>-</sup> and D<sup>-</sup> are identical. No information presently exists as to the accuracy of this assumption.

#### General comments

The strong points of the ion microprobe SIMS technique are high sensitivity, ( $\lesssim 1$  ppm in a depth profiling mode in the presence of background), minute sample consumption (10 -- 100 ng), ability to analyze all isotopes including H and D, in the same analysis if necessary, and capability for ion imaging. The major weaknesses of the techniques are the susceptibility to matrix effects (variation of ion yield with sample composition) and lack of a quantitative theory of the ion emission process. Furthermore, for many samples the development of crater surface roughness from the sputtering process can cause degradation of depth resolution. Consequently, standards are required for quantitation, and in the low concentration region (< 0.1 atom %) in which the technique excels, few quantitative techniques exist for confirmation of concentration, and certification of lateral and in-depth homogeneity of standards.

#### Observation of Lattice Damage (Ref. 13)

We approached the damage distribution by various methods. Most of the measurements were made by backscattering and channeling to profile the defect distribution (crystal damage) due to hydrogen bombardment. The results were verified by measuring the depths of blisters, and by spreading-resistance measurements on a beveled sample.

The channeling method measures the damage-distribution rather than the hydrogen distribution. But for light ions such as protons, we expect that both distributions are very similar to each other.<sup>16</sup>

Damage distributions for protons in silicon were measured by backscattering and channeling with  $^4\text{He}^+$  ions. The silicon sample was mounted on a goniometer that had three degrees of freedom: rotation, tilt, and translation. The beam was aligned with respect to the  $\langle 100 \rangle$  axis at the center part of the target.

After the beam was aligned on this center part, the target was translated by about 4 mm so that a clean beam spot (diameter about  $0.5 \text{ mm}^2$ ) was under investigation. A random spectrum was obtained by tilting the target by  $7^\circ$  and rotating the target during the run,<sup>31</sup> or alternatively at a fixed angle such as  $7^\circ$  from the  $\langle 100 \rangle$  axis and  $10^\circ$  from the  $\{111\}$  plane.

A typical set of runs is given in Fig. 24, for samples damaged by  $1 \times 10^{17}/\text{cm}^2$  protons at 40 keV. For the data acquisition,  $20 \mu\text{C}$  of 2.08 MeV helium ions backscattered at  $170^\circ\text{C}$  with incidence along the  $\langle 100 \rangle$  direction was used, and the solid angle for the scattering was 4.11 msr. The damage region is seen to be well localized at a given depth, and in the surface region of the sample the amount of damage is too small to be detected by channeling.

The spectrum of the damaged Si contains contributions from both scattering and dechanneling. To extract the damage profile, the contributions must be separated; that is, the dechanneling background must be obtained beneath the damaged spectrum. Ziegler<sup>32</sup> and Schmid<sup>33</sup> treated this type of problem by the method of Bogh.<sup>34</sup> Both their treatments require that a dechanneling model be assumed. It turns out that if the damage peak is large by comparison to the dechanneling contribution, the uncertainty in dechanneling background does not significantly influence either the position of the damage peak or the full width at half maximum--FWHM--of the damage spectrum.

For our analysis we modify Ziegler's method<sup>32</sup> by combining single scattering and multiple

scattering in the dechanneling calculation. The calculation begins with a dechanneling level for a  $^4\text{He}$  beam traversing an undamaged crystal. Any increase in the random fraction of the yield is assumed to be due to scattering from "displaced silicon atoms," and the dechanneling due to those "displaced atoms" is calculated; the amount of random fraction of the yield due to dechanneling is then subtracted from this depth and the next depth interval. The number of "equivalent displaced atoms" and their dechanneling contribution are calculated again. The procedure is continued for increasing depth until the defect-free region is reached, and then the depth distribution of the displaced atoms is obtained.

Figure 25 shows damage distribution obtained by applying this procedure to energy spectra in Fig. 24. No correction has been made for the resolution of the detecting system or for energy straggling of helium ions in silicon. Such effects lead to a correction of about 20-40 Å to the broadening of the FWHM of the extracted profile given in Fig. 25.

The defect concentration given in Fig. 25 is on a relative scale. If one translates the concentration into the equivalent number of random scattering atoms that produces the random peak and the dechanneling level given in Fig. 24, the relative scale in Fig. 25 can be considered to be the percentage of the silicon atoms randomly displaced from the lattice site. Near the maximum defect region, for example (Fig. 25), the fact that about 40% of the silicon atoms are randomly distributed off lattice site is what produces the dechanneling spectrum given in Fig. 24.

The depth scale is obtained by using the energy loss table of Ziegler and Chu.<sup>21</sup> For the incident part of the beam, channeled energy loss along the  $\langle 100 \rangle$  direction is assumed to be 80% of the value for random direction. Any localized energy loss value is a superposition of channeled and random energy loss according to the fractional amount of random atoms in silicon crystal. One can easily see in Fig. 1 that the area in front of the defect region is almost free of damage.

The  $\pm 5\%$  uncertainty in the energy loss will influence the depth scale directly. The uncertainty in the ratio of  $\langle 100 \rangle$  energy loss to random energy loss will influence it less. For example, changing this ratio from 0.6 to 1.0 (instead of 0.8, the value used in our calculation) will increase or decrease the depth by only 5%, because the outgoing path is along a random direction.

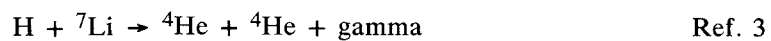
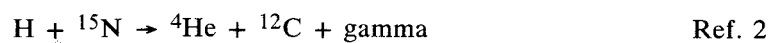
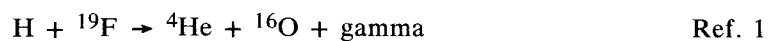
Detail study of this work is given in a separate report where we study the damage as a function of proton energy and implantation temperature (available from the authors of Ref. 13c).

### CONCLUSIONS

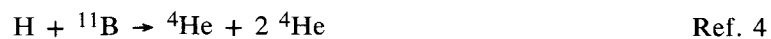
We have attempted to evaluate nine ion beam techniques which have been used to profile hydrogen in silicon. Our choice of hydrogen in silicon as a target put constraints on certain techniques which have been pointed out in the text. Brief descriptions have also been included of ion beam techniques for which this target was inappropriate. But in general we have shown that quantitative analysis of hydrogen in silicon is possible with accuracies better than 8% in total hydrogen, and in hydrogen depth profiling.

TABLE 1

## Nuclear Reaction with Gamma-Ray Detected:



## Nuclear Reaction with Product Particle Detected:



## Nuclear Forward Scattering:



## Direct Backscattering:



Observation of change in stopping power: Ref. 11

Observation of lattice location of hydrogen: Ref. 12

Observation of lattice damage: Ref. 13

Secondary Ion Mass Spectrometry (SIMS) Ref. 14

TABLE 2aTYPICAL EXPERIMENTAL CONDITIONS FOR PROTON PROFILING

Technique Ref. No. (see Table 1)	1	2	2	3	4	8	13	14	14
Ion Beam Type	<sup>19</sup> F	<sup>15</sup> N	<sup>15</sup> N	<sup>7</sup> Li	<sup>11</sup> B	<sup>35</sup> Cl	<sup>4</sup> He	<sup>40</sup> Ar	<sup>133</sup> Cs
Beam Energy (MeV)	17	7	7	3.5	2	30	2	.005	.02
Beam Current (nA)	30	50	20	450	20	9	20	1000	30
Beam Spot Size (Dia. in mm)	4	7	4	3.2	1	4	1	.07	.024
Total Charge for Profile ( $\mu$ C)	45	200	120	3000	25	38	20	900	30
Total Time for Spectrum (min.)	45	120	130	100	45	69	17	15	14
Net Counts at H peak*	843	700	650	543	1000	647	100	$5 \times 10^5$	7000
Particle Detected	$\gamma$ -ray	$\gamma$ -ray	$\gamma$ -ray	$\gamma$ -ray	$\alpha$	<sup>1</sup> H	<sup>4</sup> He	<sup>1</sup> H <sup>+</sup>	<sup>1</sup> H <sup>-</sup>
Detector Type	NaI	NaI	NaI	NaI	Si	Si	Si	SIMS	SIMS
Detector Angle	$\sim 90^\circ$	$0^\circ$	$\sim 90^\circ$	$90^\circ$	$90^\circ$	$20^\circ$	$170^\circ$	$0^\circ$	-
Detector Filter	-	-	-	-	Mylar	Mylar	-	-	-
Detector Solid- Angle (msr)	700	800	700	3100	740	0.7	4	-	-
Target Tilt from Normal to Beam	$0^\circ$	$10^\circ$	$0^\circ$	$0^\circ$	$45^\circ$	$80^\circ$	$0^\circ$	$60^\circ$	$17^\circ$
Heat into Sample (watts)	.51	.35	.14	1.58	.04	.054	.04	.005	.0008
Estimated Depth Resol. in Si (nm) FWHM at 400 nm	20	4	4	170	40	21	20	10	10

\*PROTON IMPLANTS WERE  $10^{16}$  H/cm<sup>2</sup> AT 40 keV.

TABLE 2b

TYPICAL EXPERIMENTAL CONDITIONS FOR DEUTERIUM PROFILING

Technique Ref. No. (see Table 1)	5	5	8	10	14	14
Ion Beam Type	<sup>3</sup> He	<sup>3</sup> He	<sup>35</sup> Cl	<sup>1</sup> H	<sup>40</sup> Ar	<sup>133</sup> Cs
Beam Energy (MeV)	.75	.75	30	2.5	.011	.02
Beam Current (nA)	30	30	6	15	10	30
Beam Spot Size (Dia. in mm)	1	1	4	1	.005	.024
Total Charge for Profile ( $\mu$ C)	224	544	45	20	33	30
Total Time for Spectrum (min.)	120	300	125	20	45	14
Net Counts at H peak*	18	35	1250	330	1600	$6 \times 10^4$
<hr/>						
Particle Detected	$\alpha$	$\alpha$	<sup>2</sup> H	<sup>1</sup> H	<sup>2</sup> H <sup>+</sup>	<sup>2</sup> H <sup>-</sup>
Detector Type	Si	Si	Si	Si	SIMS	SIMS
Detector Angle	50°	110°	20°	164°	-	-
Detector Filter	-	-	Mylar	-	-	-
Detector Solid- Angle (msr)	.04	.04	0.4	.31	-	-
Target Tilt from Normal to Beam	60°	0°	80°	0°-60°	0°	17°
<hr/>						
Heat into Sample (watts)	.02	.02	.036	.037	.0001	.0008
Estimated Depth Resol. in Si (nm) FWHM at 400 nm	23	60	15	98-21	12	10

\*DEUTERON IMPLANTS WERE  $10^{17}$  D/CM<sup>2</sup> AT 31 keV.

TABLE 3

Depth Assignments for H and D round-robin samples using SIMS.

	<u>H(40 keV)</u>	<u>D(31 keV)</u>
$R_p$	$3880 \pm 50 \text{ \AA} \text{ (Cs}^+)$	$3990 \pm 50 \text{ \AA} \text{ (Cs}^+)$ *
	$3965 \pm 100 \text{ \AA} \text{ (Ar}^+)$	$5000 \text{ \AA} \text{ (Ar}^+)$ †
FWHM	$1010 \pm 50 \text{ \AA} \text{ (Cs}^+)$	$1410 \pm 50 \text{ \AA} \text{ (Cs}^+)$
	$1000 \pm 100 \text{ \AA} \text{ (Ar}^+)$	$1800 \text{ \AA} \text{ (Ar}^+)$ †

\* An independent check of this depth assignment was made using a calibrated Talysurf. This measurement gave  $R_p = 3965 \pm 50 \text{ \AA}$ .

† Depth was determined from established sputtering rates without post-measurement of crater depth.

REFERENCES

- Ref. 1. a) D.A. Leich and T.A. Tombrello, Nucl. Inst. and Meth. 108, 67 (1973).  
b) J. Bottiger, J.R. Leslie and N. Rud, Jour. Appl. Phys. 47, 1672 (1976).  
c) S.T. Picraux, J. Bottiger and N. Rud, J. Nuclear Matl. 63, 110 (1976).  
d) S.T. Picraux, J. Bottiger and N. Rud, Appl. Phys. Lett. 28, 179 (1976).  
e) G.J. Clark, C.W. White, D.D. Allred, and B.R. Appleton, Nucl, Inst. and Meth. (this issue).
- Ref. 2. a) W.A. Lanford, H.P. Trautvetter, J.F. Ziegler and J. Keller, Appl. Phys. Lett., 28, 566 (1976).
- Ref. 3. a) P.N. Adler, E.A. Kamykowski and G.M. Padawer, pg. 623, "Hydrogen in Metals," Amer. Soc. for Metals (1974).  
b) G.M. Padawer, E.A. Kamykowski, M.C. Stauber, M.D. D'Agostino, W. Brandt, pg. 1919, Proc. of 5<sup>th</sup> Lunar Science Conf (1974), Geochim. Cosmocim. Acta, Suppl. 5, Vol. II, Pergamon Press, New York, 1974.  
c) P.N. Adler, G.M. Padawer, E.A. Kamykowski, Proc. of Tri-Service Corrosion of Military Equipt., Vol. 2, AFML-TR-75-42. Copies may be obtained from the authors.
- Ref. 4. a) E. Ligeon and A. Guivarc'h, Radiation Eff. 22, 101 (1974).  
b) E. Ligeon and A. Guivarc'h, Radiation Eff. 27, 129 (1976).  
c) A. Tuross, L. Wielunski and A. Barcz, Nucl. Inst. and Meth. 113, 605 (1973).
- Ref. 5. a) P.P. Pronko and J.G. Pronko, Phys. Rev. 9B, 2870 (1974).  
b) R.A. Langley, S.T. Picraux and F.L. Vook, J. Nucl. Mat. 53, 257 (1974)  
c) J. Bohdanský, J. Roth, and W.P. Poschenrieder, "Int. Conf. of Applications of Ion Beams to Materials", 25, The Institute of Physics, London, (1975), pg. 307.  
d) W. Eckstein, R. Behrisch, and J. Roth, "Ion Beam Surface Layer Analysis", Vol. 2, Plenum Press, New York (1976).  
e) Y.L. Yarnell, R.H. Lovberg, W.R. Stratton, Phys. Rev. 90, 292 (1953).

- f) B.M.U. Scherzer, H. Bay, R. Behrisch, P. Brogersen, and J. Roth, Nucl. Inst. and Meth. (this issue).
- g) B.M.U. Scherzer, R. Behrisch, W. Eckstein, U. Littmark, J. Roth, and M.K. Sinha, J. Nucl. Matl. 63, 100 (1976).
- Ref. 6. a) P.B. Johnson, Nucl. Inst. and Meth. 114, 467 (1974).
- b) W. Möller, J. Appl. Phys. 48, 893 (1977).
- Ref. 7. a) Y.Y. Chu and L. Friedman, Nucl. Inst. and Meth. 38, 254 (1965).
- b) H.W. Lefevre, J.D. Anderson, J.C. Davis (to be published in IEEE), Conf. on Use of Small Accelerators (1976).
- c) R.L. Maclin and J.H. Gibbons, Phys. Rev. 109, 105 (1958).
- d) J.C. Davis and J.D. Anderson, J. Vac. Sci. Tech. 12, 358 (1975).
- e) J.C. Overley and H.W. Lefevre, Advances in Chem. Series - Radiation Effects on Solid Surfaces (1976).
- Ref. 8. a) J. L'Ecuyer, C. Brassard, C. Cardinal, J. Chabbal, L. Deschenes, J.P. Labrie, B. Terreault, J.G. Martel and R. St-Jacques, Jour. Appl. Phys. 47, 381 (1976).
- b) B. Terreault, J.G. Martel, R.G. St-Jacques, J.L'Ecuyer, J. Vac. Sci. Technol. 14, 492 (1977).
- c) J. L'Ecuyer, C. Brassard, C. Cardinal, and B. Terreault, Nucl. Inst. and Meth., (this issue).
- Ref. 9. a) B.L. Cohen, C.L. Fink and J.D. Degnan, Jour. Appl. Phys. 43, 19 (1972).
- Ref. 10. The following refer mostly to He profiling but are applicable to D or T profiling:
- a) R.S. Blewer, Jour. Nucl. Materials 53, 268 (1974).
- b) R.S. Blewer, Appl. Phys. Lett. 23, 593 (1973).
- c) R.S. Blewer, pg. 525, Vol. II, U.S. Natl. Tech. Info. Serv., CONF-740402-P2," Conf. on Technolgy of Controlled Nuclear Fusion."
- d) R.S. Blewer, Nucl. Inst. and Meth. (this issue).

- e) R.S. Blewer, pg. 185, "Ion Beam Surface Layer Analysis", Plenum Press, New York (1976).
- Ref. 11. These references refer to He, but are applicable to H profiling:
- a) J. Roth, R. Behrisch and B.M.U. Scherzer, Appl. Phys. Lett. 25, 643 (1974).
  - b) J. Roth, R. Behrisch and B.M.U. Scherzer, pg. 573, "Applications of Ion Beams to Metals," Plenum Press (1973).
- Ref. 12.
- a) S.T. Picraux, pg. 527, "Ion Beam Surface Layer Analysis," Plenum Press (1976).
  - b) H.D. Carstanjen, *ibid*, pg. 497.
  - c) H.D. Carstanjen and R. Sizmann, Phys. Lett., 40A, 93 (1972).
  - d) J.L. Whitton, J.B. Mitchell, T. Schober and H. Wenzl, Acta. Metall. 24, 483 (1976).
- Ref. 13.
- a) R. Behrisch and J. Roth, pg. 539, "Ion Beam Surface Layer Analysis," Plenum Press (1976).
  - b) D.A. Thompson and S.E. Robinson, Nucl. Inst. and Meth., 131, (1976).
  - c) W.K. Chu, R.H. Kastl, R.F. Lever, S. Mader and B.J. Masters, "Conf. on Ion Implantation in Semiconductors and other Materials", 1977.
- Ref. 14.
- a) H. Liebl, Int. J. Mass. Spectr. Ion Phys., 6, 401 (1971).
  - b) W.O. Hofer, H. Liebl, G. Roos, and G. Staudenmeier, Int. J. Mass. Spectr. Ion Phys., 13, 327 (1976).
  - c) P. Williams, R.K. Lewis, C.A. Evans, Jr., and P.R. Hanley. Analytical Chemistry, In Press (August 1977).
  - d) P. Williams, C.A. Evans, Jr., M.L. Grossbeck and H.K. Birnbaum, Analytical Chemistry, 48, 964, (1976).
  - e) R.W. Linton, A. Loh, D.F.S. Natusch, C.A. Evans, Jr., and P. Williams, Science, 191, 852, (1976).
  - f) P. Williams and C.A. Evans, Jr., Appl. Phys. Lett. 30, 559, (1977).

- g) C.A. Evans, Jr., National Bureau of Standards Spec. Publ. 400-23 (A.G. Lieberman, Ed.), p. 219, (1976).
- Ref. 15. Silicon wafers were supplied by IBM Corporation, S.P. Div., East Fishkill, New York.
- Ref. 16. H.H. Andersen and J.F. Ziegler, "Hydrogen Stopping Powers and Ranges in All Elements", Pergamon Press (1977). The straggling calculations quoted differ from those in this book, and are based instead on LSS formalism calculations of J.F. Ziegler.
- Ref. 17. O.S. Oen and M.T. Robinson, Jour. Nuclear Matl. 63, 210 (1976), and W. Eckstein, F.E.P. Matschke, H. Verbeek, J. Nuclear Matl., 63, 199 (1976).
- Ref. 18. L.C. Northcliffe and R.F. Schilling, Nucl. Data Tables A1, 233 (1970).
- Ref. 19. D.J. Whitehouse, pg. 53 in "Characterization of Solid Surfaces", ed. by Kane and Larabee, Plenum Press, New York (1974).
- Ref. 20. B. Maurel, D. Dieumegard, and G. Amsel, pg. 71, Catania Working Data, unpublished.
- Ref. 21. J.F. Ziegler and W.K. Chu, Atomic and Nuclear Data Tables, 13, 463 (1974).
- Ref. 22. J. Lindhard and A. Winther, Mat. Fys. Medd. Dan. Vid. Selsk. 34, No. 4 (1964).
- Ref. 23. R.K. Nesbet and J.F. Ziegler (to be published).
- Ref. 24. J.P. Longequene, PhD Thesis, Grenoble University, France (unpublished).
- Ref. 25. J.S. Forster, D. Ward, H.R. Andrews, G.C. Ball, G.J. Costa, W.G. Davies, and I.V. Mitchell, Nucl. Inst. and Meth., 136, 349 (1976).
- Ref. 26. J.F. Ziegler, Nucl. Inst. and Meth. (this issue).
- Ref. 27. R.S. Blewer, Appl. Phys. Lett. 23, 593 (1973).
- Ref. 28. A. Feuerstein, H. Grahmann, S. Kalbitzer, and H. Oetzmann, p. 471, "Ion Beam Surface Layer Analysis", Plenum Press, New York (1976).
- Ref. 29. E. Bogh, Rad. Eff. 12, 13 (1972).
- Ref. 30. D.C. Kocher and T.B. Clegg, Nucl. Phys. A132, 455 (1969).

- Ref. 31. J.F. Ziegler and B.L. Crowder, *Appl. Phys. Lett.*, 20, 178 (1972); Errata: *Appl. Phys. Lett.*, 22, 347 (1973).
- Ref. 32. J.F. Ziegler, *J. Appl. Phys.* 43, 2973 (1972).
- Ref. 33. D. Schmid, *Rad. Eff.* 17, 201 (1973).
- Ref. 34. E. Bogh, *Can. J. Phys.* 46, 653 (1968).
- Ref. 35. C.W. Magee and C.P. Wu, *Nucl. Inst. and Meth.* (this issue).
- Ref. 36. P. Williams, R.K. Lewis, C.A. Evans Jr., and P.R. Hanley, *Nucl. Inst. and Meth.* (this issue).

APPLICATIONS OF HYDROGEN PROFILING (See also Ref. 1-14)

1. Quantitative Analysis of Hydrogen in Glow Discharge Amorphous Silicon  
M.H. Brodsky, M.A. Frisch, J.F. Ziegler and W.A. Lanford  
Applied Phys. Letts. 30, (1977) 561.
2. Glass Hydration: A Method of Dating Glass Objects  
W.A. Lanford  
Science 196 (1977) 975.
3. Hydrogen Surface Contaminations and Containment of Ultra-Cold Neutrons  
W.A. Lanford, K. Davis, P. LaMarche, R. Golub  
Bull. Am. Phys. Soc. 22 (1977) 549.
4. Location of H and D impurities in Al single crystals. J.P. Bugeat, A.C. Cherni, and E. Ligeon, Phys. Lett. 58A, 127 (1976).
5. Hydrogen and Deuterium Implantation to Investigate some Aspects of the Defect-Impurity Interactions in Metals. E. Ligeon, J.P. Bugeat, A.C. Chemi, Nucl. Inst. and Meth. (this issue).
6. "Measurement of the Distribution of Light Impurities in First-Wall Materials: He in Nb", B. Terreault, J.G. Martel, R.G. St-Jacques, G. Villeux, J. L'Ecuyer, C. Brassard, C. Cardinal, L. Deschênes, and J.P. Labrie, J. Nucl. Mater, 63, 106 (1976).  
Profiles of 10 keV Helium at high doses (up to  $6 \times 10^{18}$  He/cm<sup>2</sup>) in niobium, show reemission through the surface.
7. "Low Energy Helium Bombardment of Copper and Niobium: Gas Depth Profile Measurements",  
B. Terreault, J.G. Martel, R.G. St-Jacques, G. Veilleux, J. L'Ecuyer, C. Brassard, C. Cardinal, L. Deschênes and J.P. Labrie, Proc. 9th Symposium on Fusion Technology (Pergamon, Oxford, 1976).  
Profiles of 5, 10, 15, 20 and 25 keV Helium in copper are measured and found in reasonable agreement with theory.

8. "Penetration of Hydrogen into Aluminum on Exposure to Water", H. Leidheiser and N. Das, Jour. Electrochem. Soc. 122, 641 (1975).
9. "Helium Depth Profiles in Thin Metal Foils", L. Shabason, and W.J. Choyke, Nucl. Instr. Meth. 138, 533 (1976).
10. J. Bottiger, S.T. Picraux, N. Rud, and T. Laursen, J. Appl. Phys. 48, 920 (1977).
11. "Depth Distribution and Migration of Helium in Vanadium at Elevated Temperatures", R.S. Blewer and R.A. Langley, Jour. Nucl. Mat'l. 63, 337 (1976).

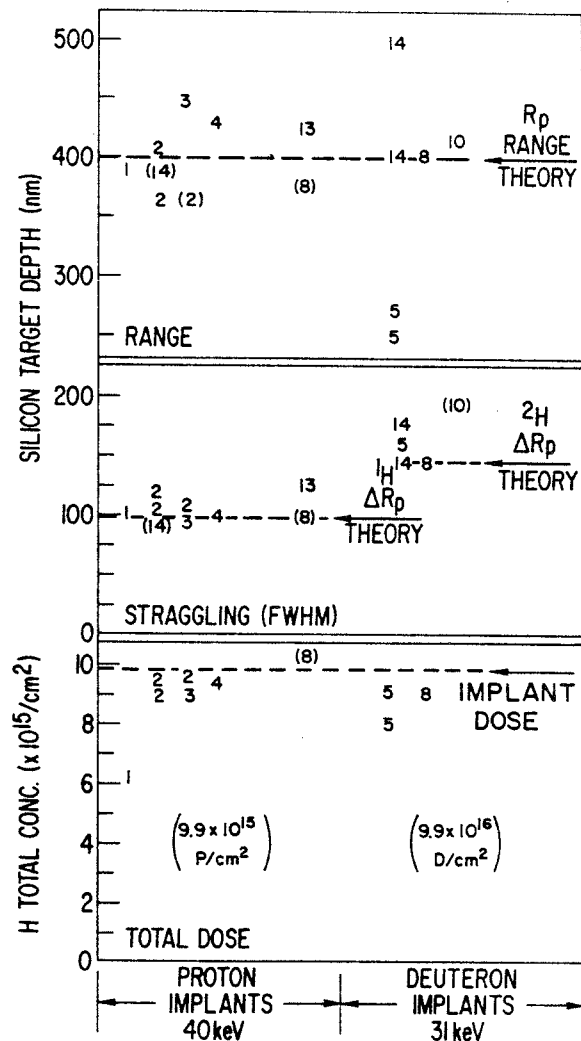


Figure 1. Shown are the results of various techniques applied to profiling hydrogen in silicon. The hydrogen was ion implanted at the energies shown to produce a hydrogen peak about 400 nm below the silicon surface. The upper portion of this figure shows the Range (location of the H peak) as determined by each method. The middle portion of this figure shows the stragglings of the H distribution, defined as the width of the H peak (FWHM). The lower portion shows the total H concentration measured in the sample. Where values are missing (such as number 6 in the lower plot) it is due to that technique being inapplicable to that measurement (see text for details). All numbers in the same vertical column were measurements on the same sample (some samples were cut into several pieces). Numbers in parenthesis indicate a second measurement on the same sample (these samples may have been subjected to anomalous redistribution of hydrogen during the first analysis). The numbers correspond to the references of the ion beam techniques (see Table 1).

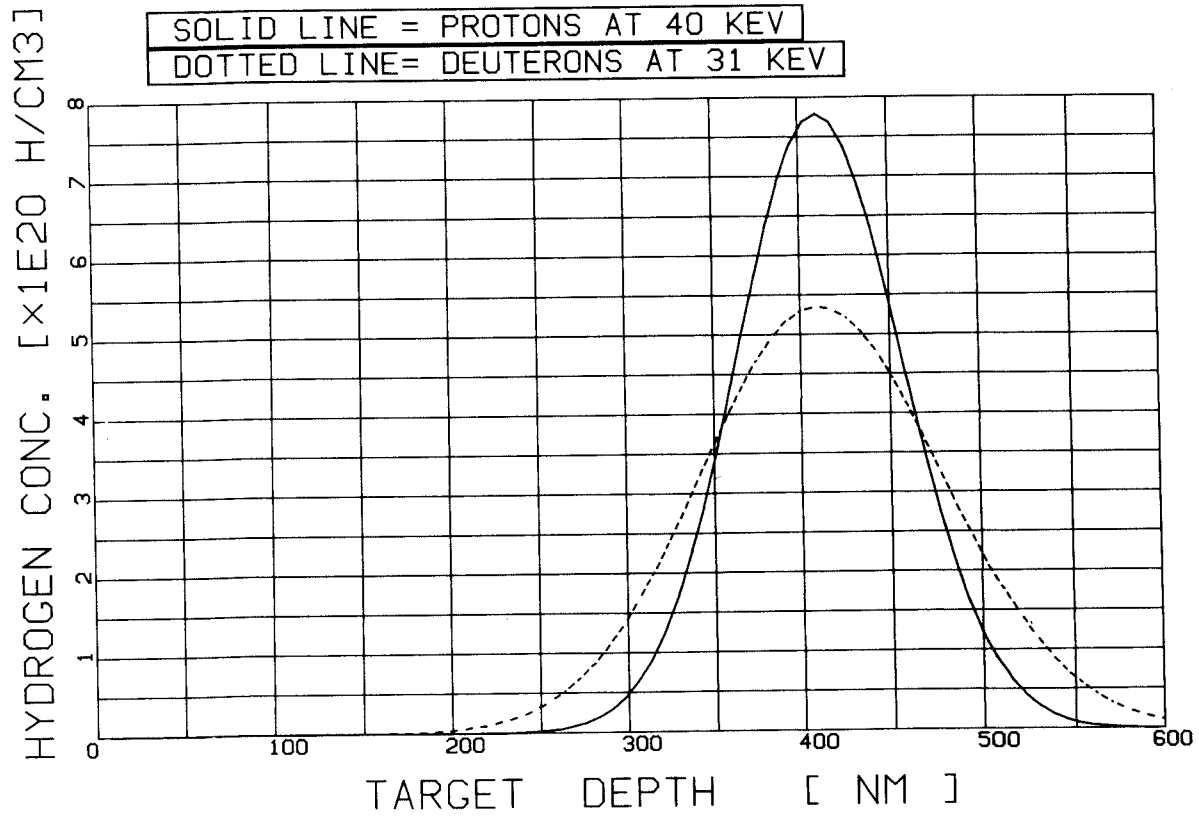
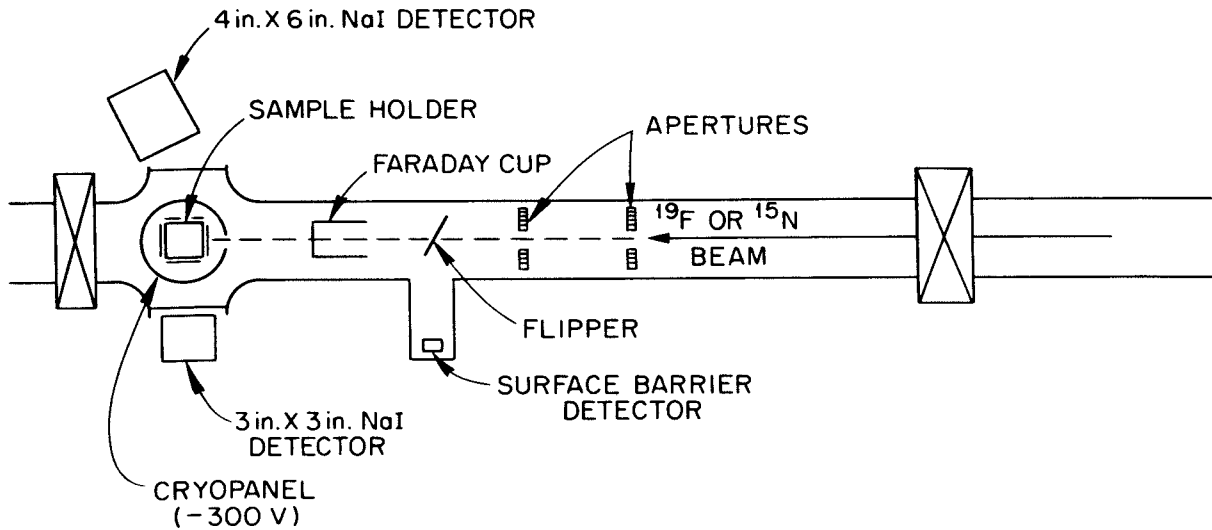


Figure 2. Composite schematic of the profile of protons and deuterons ion implanted into amorphous Si at the energies shown. The profiles represent the average of the 16 analysis experiments reported in this paper. The total hydrogen dose was nominally  $10^{16}$  H/cm<sup>2</sup>, but the actual implanted dose was  $9.9 \times 10^{15}$  H/cm<sup>2</sup> when reflected H is taken into account (the deuteron implants were actually  $10^{17}$  D/cm<sup>2</sup> and were normalized to  $10^{16}$  D/cm<sup>2</sup>).



Experimental Apparatus for Hydrogen Depth Profiling.

Figure 3. Typical experimental apparatus for the profiling of H in materials using techniques where a  $\gamma$ -ray is emitted (see Ref. 1-3). Good vacuum conditions are desirable to prevent hydrocarbon build-up on the target surface. In this setup a cryopanel surrounds the target. The  $\gamma$ -rays from the three techniques in Ref. 1-3 are all believed to be isotropic, so the NaI detectors can be placed at any convenient position.

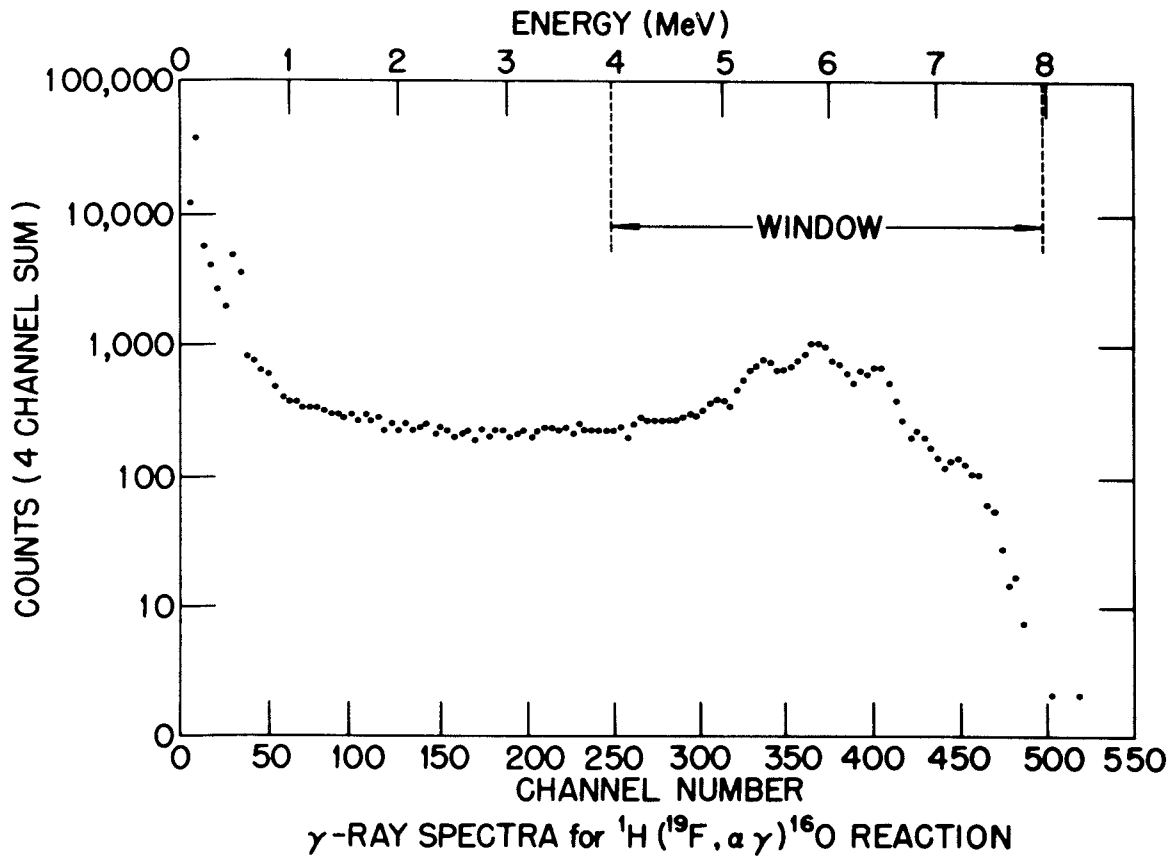
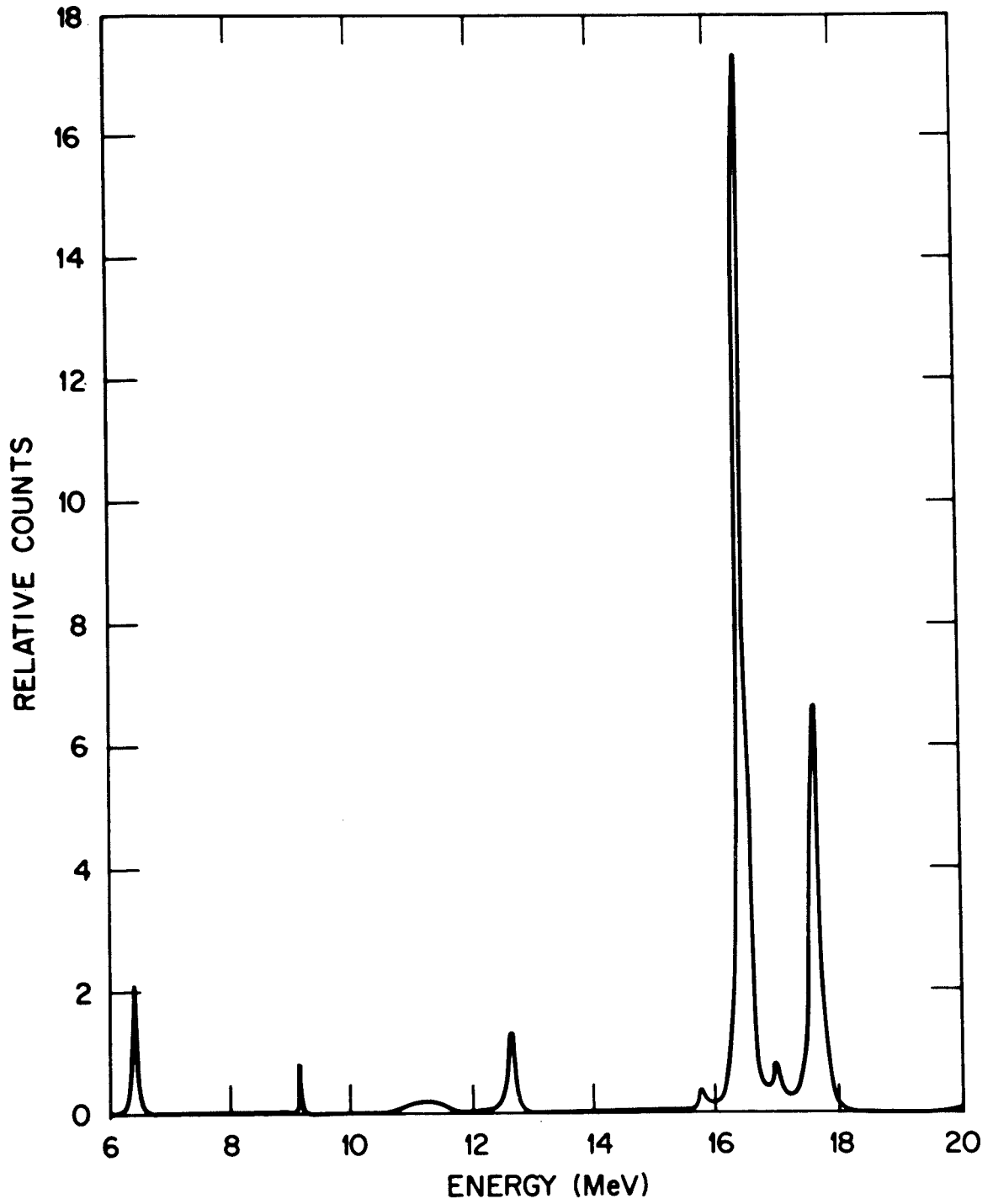


Figure 4. Gamma-ray spectrum from the nuclear reaction  ${}^{19}\text{F}$  ( $\sim 17$  MeV) +  ${}^1\text{H}$ . The dashed lines indicate the counting window. The various peaks correspond to full  $\gamma$ -ray energy, and the first and second escape peaks. The high energy background is mostly due to cosmic rays and is normally removed from spectra (this background is time-dependent).



Excitation Function for  ${}^1\text{H}({}^{19}\text{F}, \alpha \gamma){}^{16}\text{O}$ .

Figure 5. Excitation function for the  ${}^1\text{H}({}^{19}\text{F}, \alpha, \gamma){}^{16}\text{O}$  nuclear reaction for  ${}^{19}\text{F}$  energies of 6-20 MeV. (Curve taken from Ref. 20).

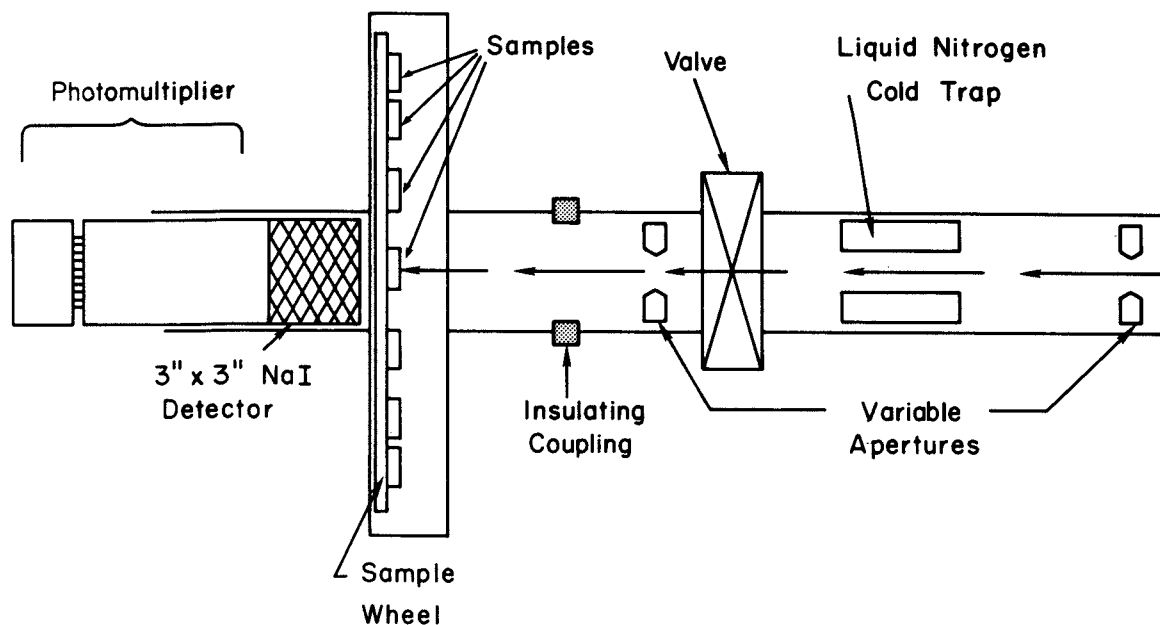


Figure 6. Typical experimental apparatus for the profiling of H in materials using techniques where high energy  $\gamma$ -rays are emitted (see Ref. 1-3). In this setup the  $\gamma$ -ray detector is placed directly behind the targets to maximize the detector solid-angle. The entire target chamber is electrically isolated and acts as a Faraday Cup. Since the techniques of Ref. 1-3 demand a change of accelerator energy for each data point, many targets may be remotely rotated into the ion beam for each ion energy.

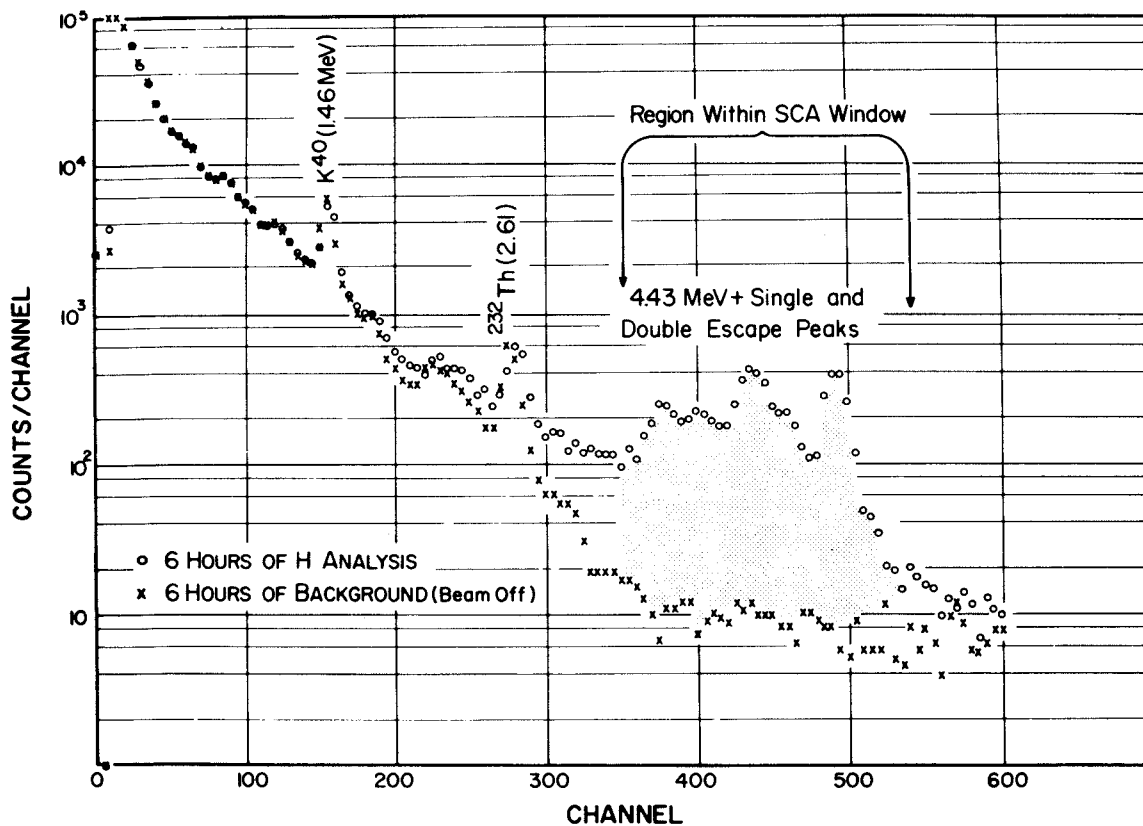


Figure 7. Gamma-ray spectra recorded with the NaI detector for the setup shown in Fig. 6. Two spectra are shown both accumulated for 6 hours, one with beam on and one with beam off. The region counted when hydrogen profiling is shown. It includes the full energy (4.43 MeV) peak, the two escape peaks and part of the Compton Scattering peak.

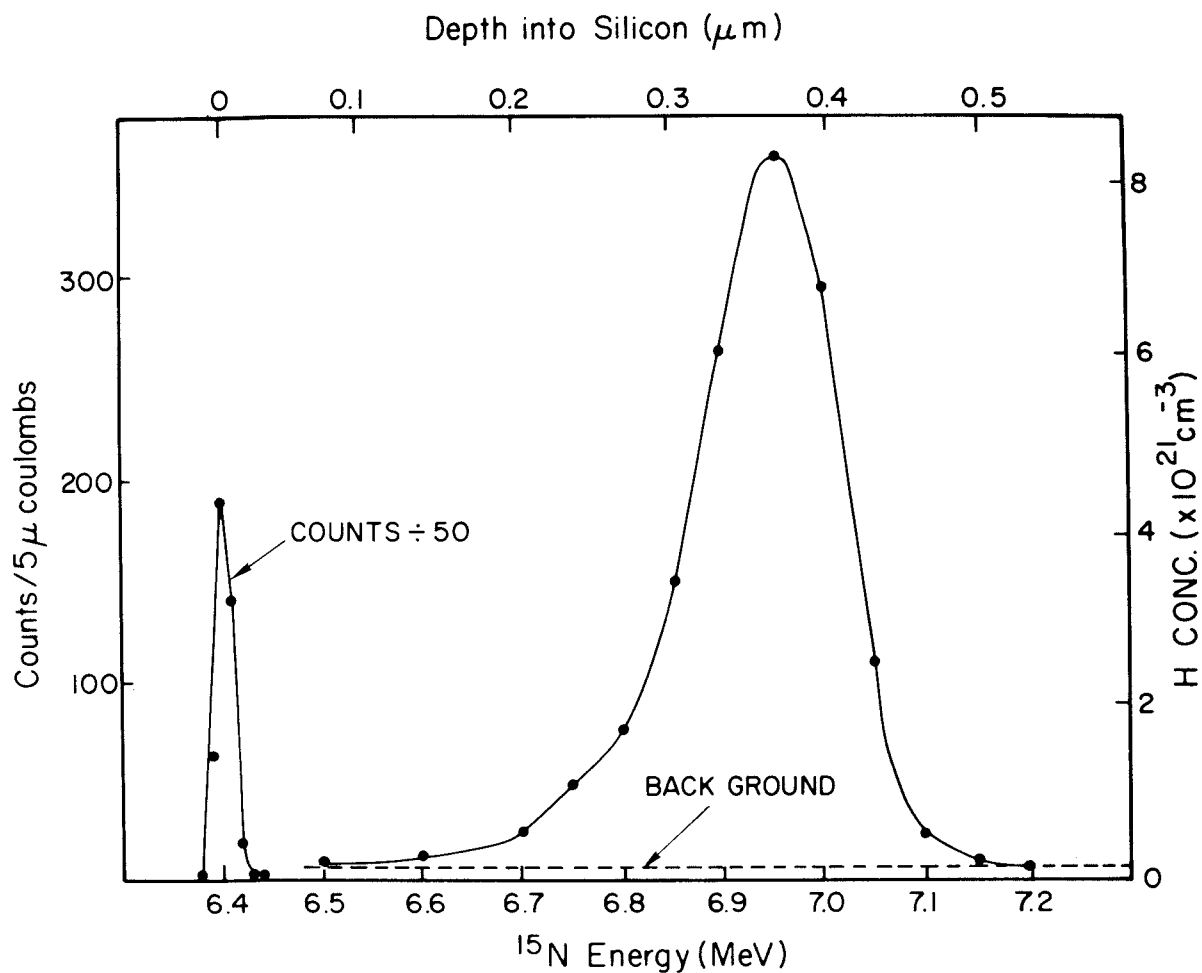


Figure 8. The hydrogen profile of a silicon wafer implanted with  $10^{16}$  H/cm<sup>2</sup> at 40 keV. Shown is the data as recorded (yield vs. beam energy) with the background shown. The top and right axes show the corresponding depth and concentration scales. The peak on the left comes from hydrogen surface contaminations.

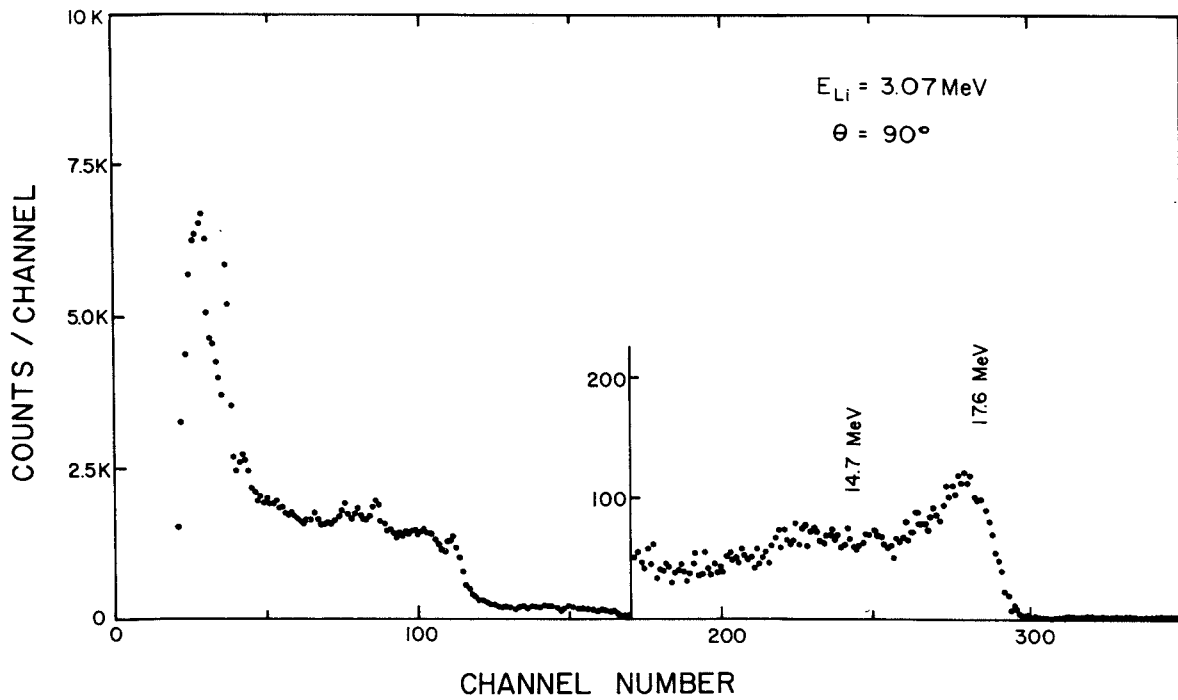


Figure 9. A typical NaI pulse height gamma ray spectrum from a 3.07 MeV  ${}^7\text{Li}$  ion beam on a N.B.S. Hydrogen in Titanium reference sample. The  ${}^1\text{H}_1 ({}^7\text{Li}, \gamma) {}^8\text{Be}$  resonance reaction populates the 17.6 MeV state in  ${}^8\text{Be}$  which can decay directly to the ground state via emission of 17.6 MeV gamma rays or to a very broad state at 2.90 MeV via emission of gamma rays of approximately 14.7 MeV.

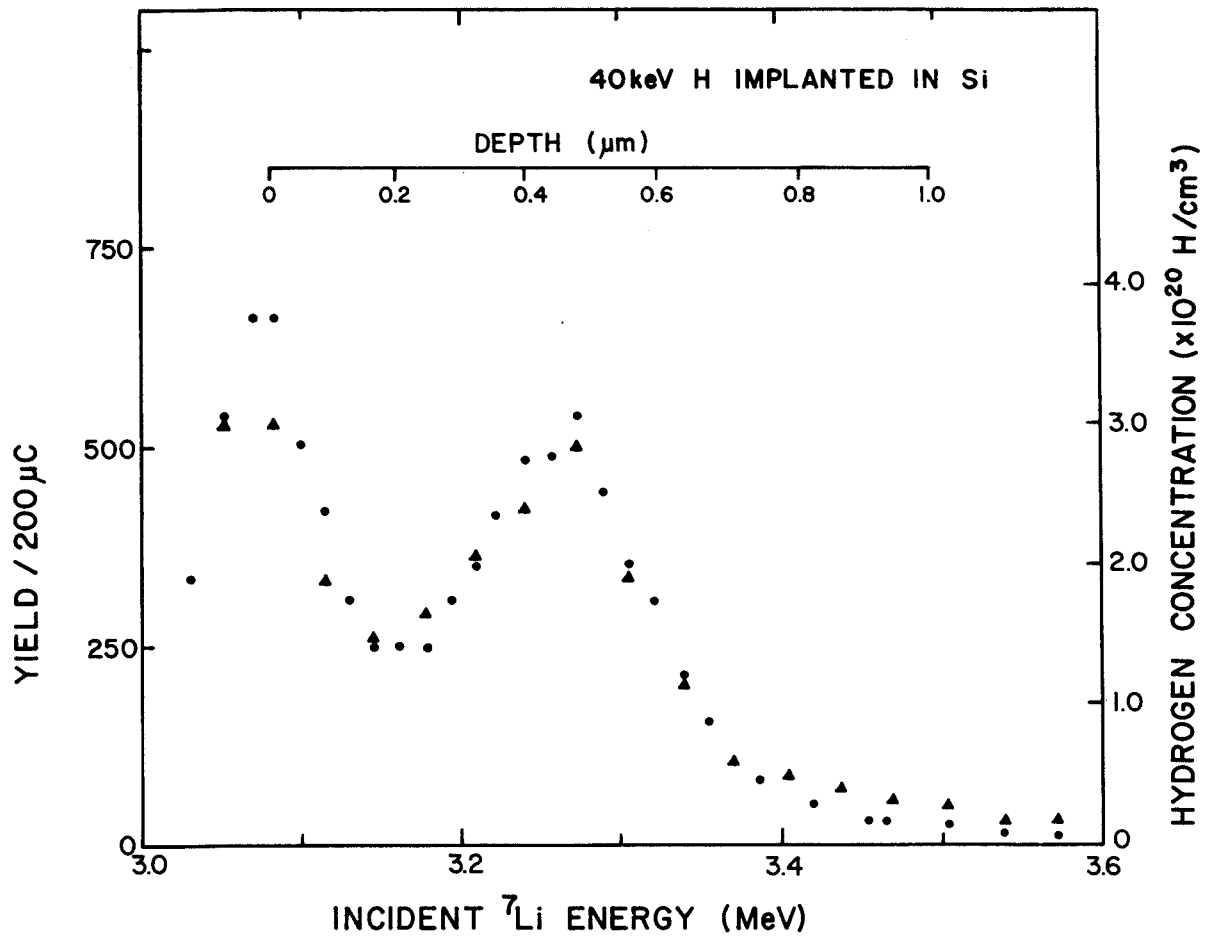


Figure 10. Experimental yield curve of the  ${}^1\text{H}+{}^7\text{Li}$  (3.07 MeV)  $\rightarrow$   $\gamma$ -ray from the proton round-robin sample. Results are shown for two separate measurements calibrated with different sets of hydrogen-in-titanium standards. The resonance width of the reaction, a depth resolution of 170 nm, has not been extracted from the profile.

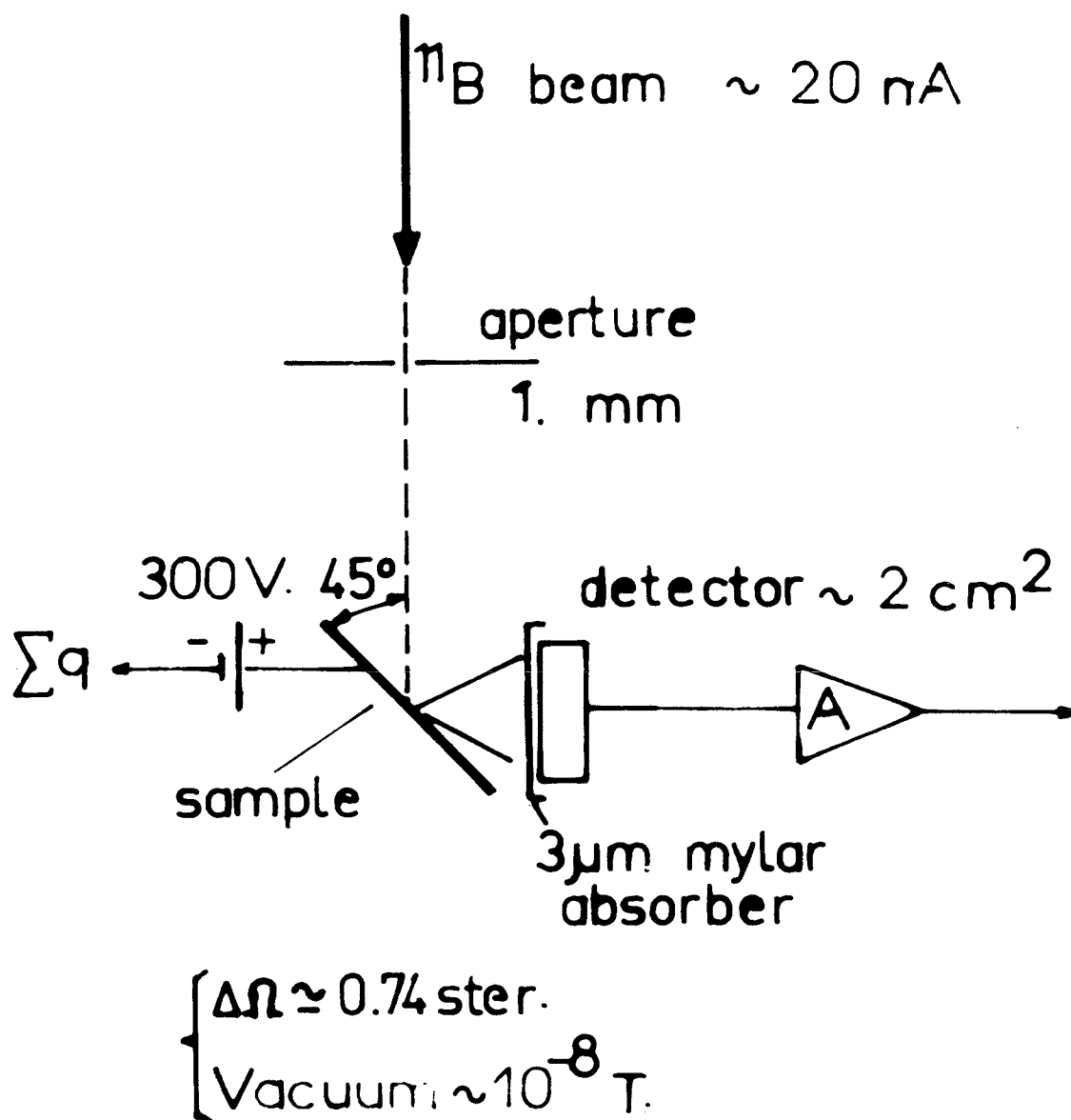


Figure 11. Diagram of the experimental apparatus for profiling H in materials using  $^{11}\text{B}$  ions at  $\sim 2 \text{ MeV}$ , and detecting the product  $\alpha$ -particles. The mylar absorber is necessary to prevent the detector from being saturated by elastically scattered  $^{11}\text{B}$  ions.

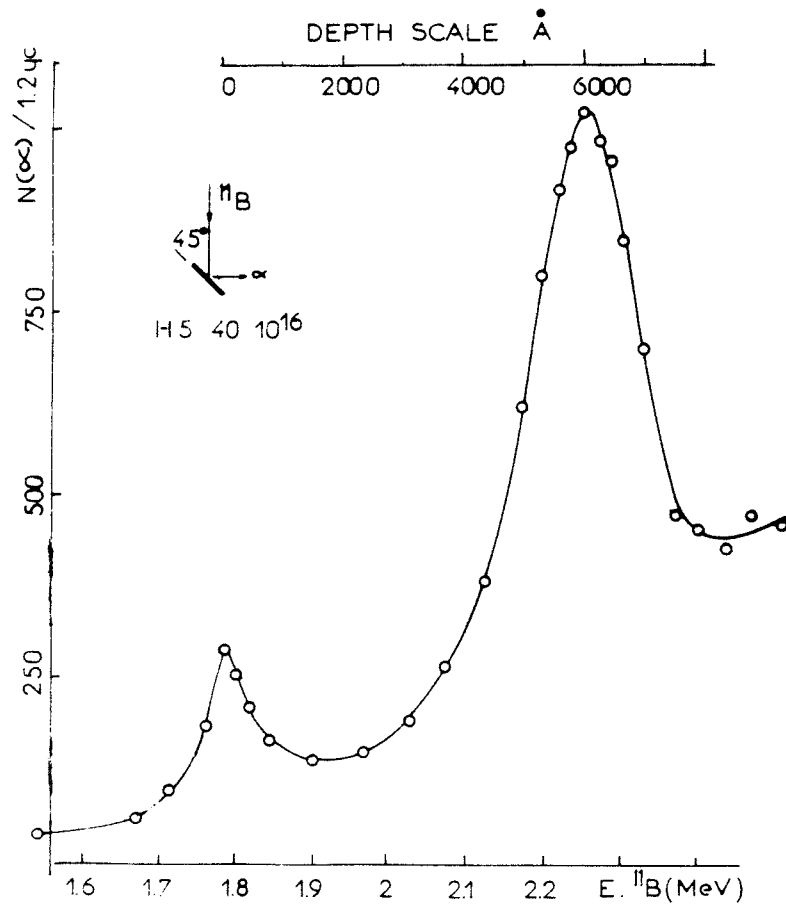


Figure 12. Experimental yield curve of the  ${}^1\text{H} + {}^{11}\text{B}$  ( $\sim 2$  MeV)  $\rightarrow \alpha + 2 \alpha$  reaction from the proton round-robin sample (average of three different curves plotted from three different runs). The incoming  ${}^{11}\text{B}$  beam energy (lower scale) is established by assuming that the resonance energy for the surface layer takes place at 1793 keV. The equivalent depth in the sample (upper scale) is established by assuming an  $dE/dx = 810 \text{ keV}/\mu\text{m}$ . The sample is tilted of  $45^\circ$  and consequently the depth scale and also  $R_p$ ,  $\Delta R_p$  etc...) is increased by a  $\sqrt{2}$  factor.

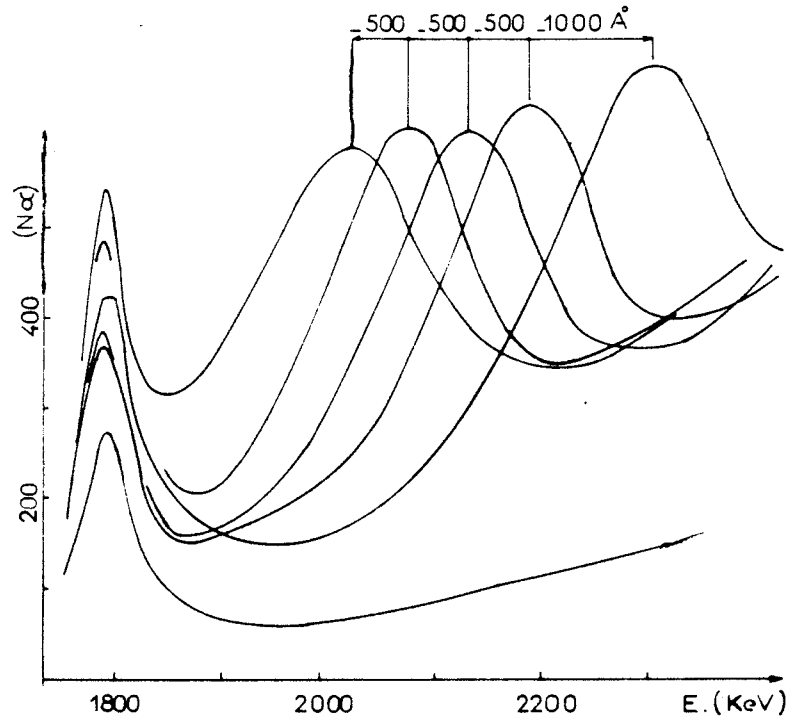


Figure 13. Yield curves of the  ${}^1\text{H} + {}^{11}\text{B} \rightarrow \alpha + 2\alpha$  nuclear reaction plotted for the silicon sample after removing by anodic oxidation layers with 0, 1000, 1500, 2000, and 2500 Å thickness. The lower curve corresponds to an unimplanted sample. The thickness of the removed layer has been checked with a "Tallystep System" and the corresponding energy loss is equal to 810 keV/ $\mu\text{m}$ . No evidence for an increase of the width of the implanted H peak caused by the straggling of the  ${}^{11}\text{B}$  beam was found.

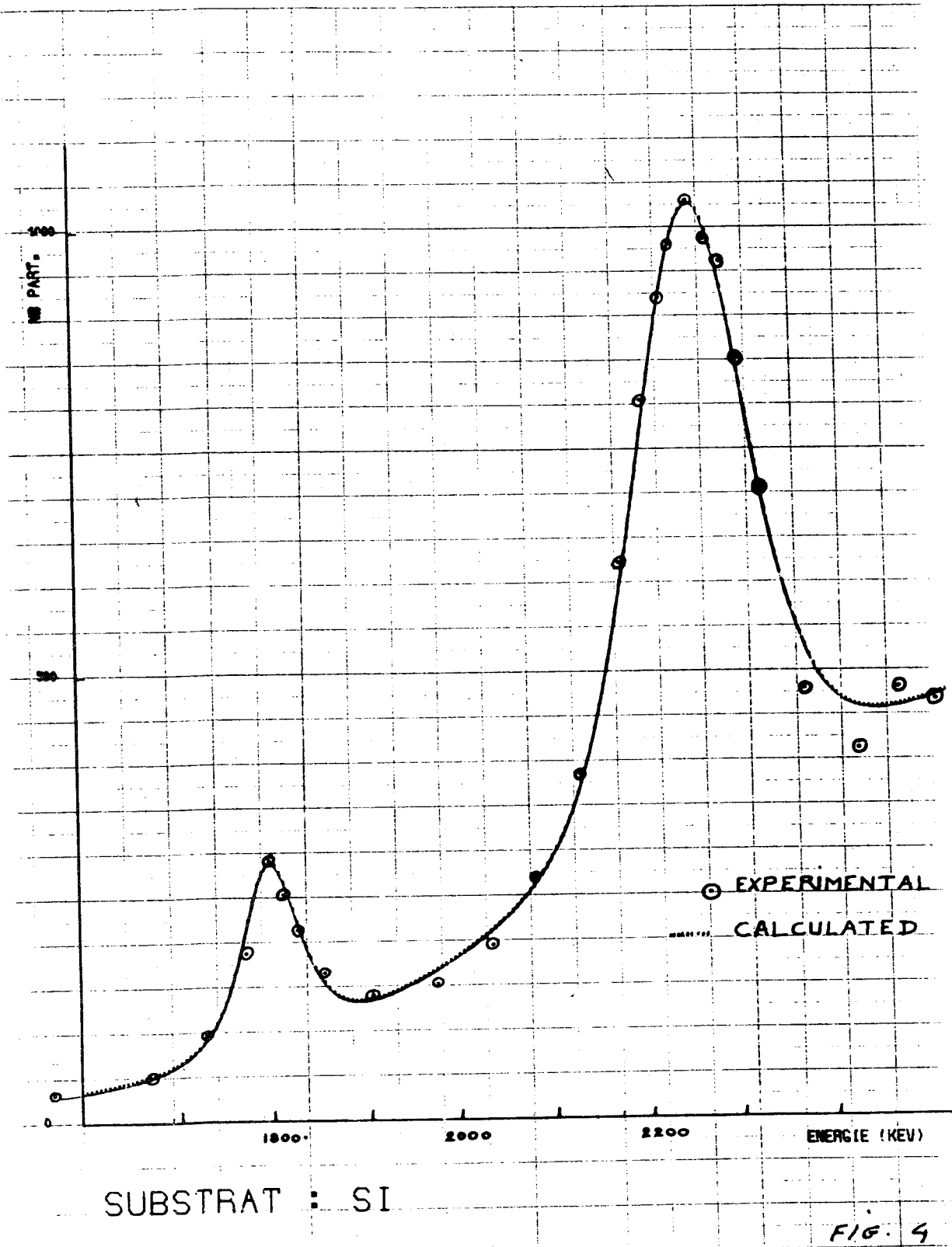
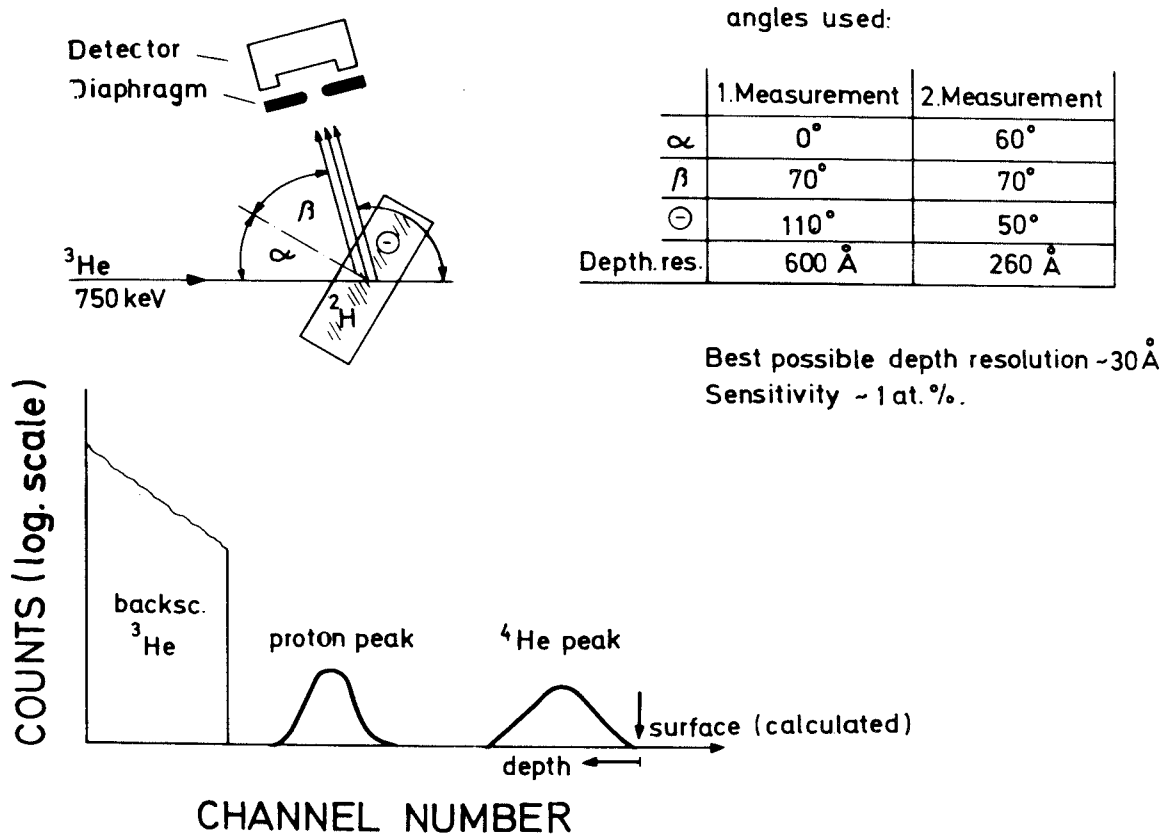


Figure 14. Comparison between experimental (○) and computed yield curve. The data used for the fit is a Hydrogen Gaussian with  $R_p = 4300 \sqrt{2} \text{ \AA}$  and  $\sigma = 440 \sqrt{2} \text{ \AA}$  (sample  $45^\circ$  tilted). The procedure for these calculations is found in Ref. 4a, 4b.

## DEUTERIUM PROFILING



**Figure 15.** The experimental setup for the profiling of D in materials is shown in the upper left. The product particles of the nuclear reaction are  ${}^4\text{He}$  ( $\sim 2.5 \text{ MeV}$ ) and protons ( $\sim 15 \text{ MeV}$ ). In the data spectrum shown at the bottom the energetic proton peak is shown at lower energy than the  ${}^4\text{He}$  peak because these protons lose only a small portion of their energy in the depletion region of the detector. Thus this proton peak position will be very sensitive to detector bias. The  ${}^4\text{He}$  count rate is very low due to the flood of elastically scattered  ${}^3\text{He}$  ions. Filters placed between the target and detector can reduce these  ${}^3\text{He}$  counts, but only at the sacrifice of some depth resolution.

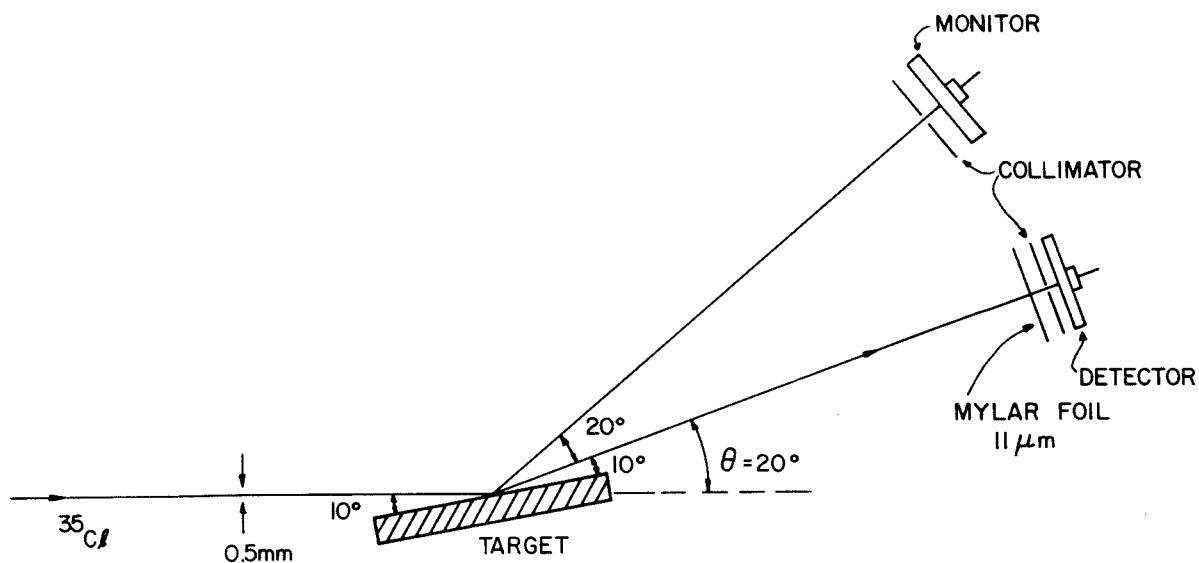


Figure 16. Experimental setup for analysing H in materials using  $^{35}\text{Cl}$  ( $\sim 30\ \text{MeV}$ ) and detecting the light mass atoms recoiling from the target. The glancing angle of the incident ions and the outgoing particles requires accurate geometric positioning. Typically the distance from the target to the detectors is 20 cm, with the detector collimated down to 1 mm width.

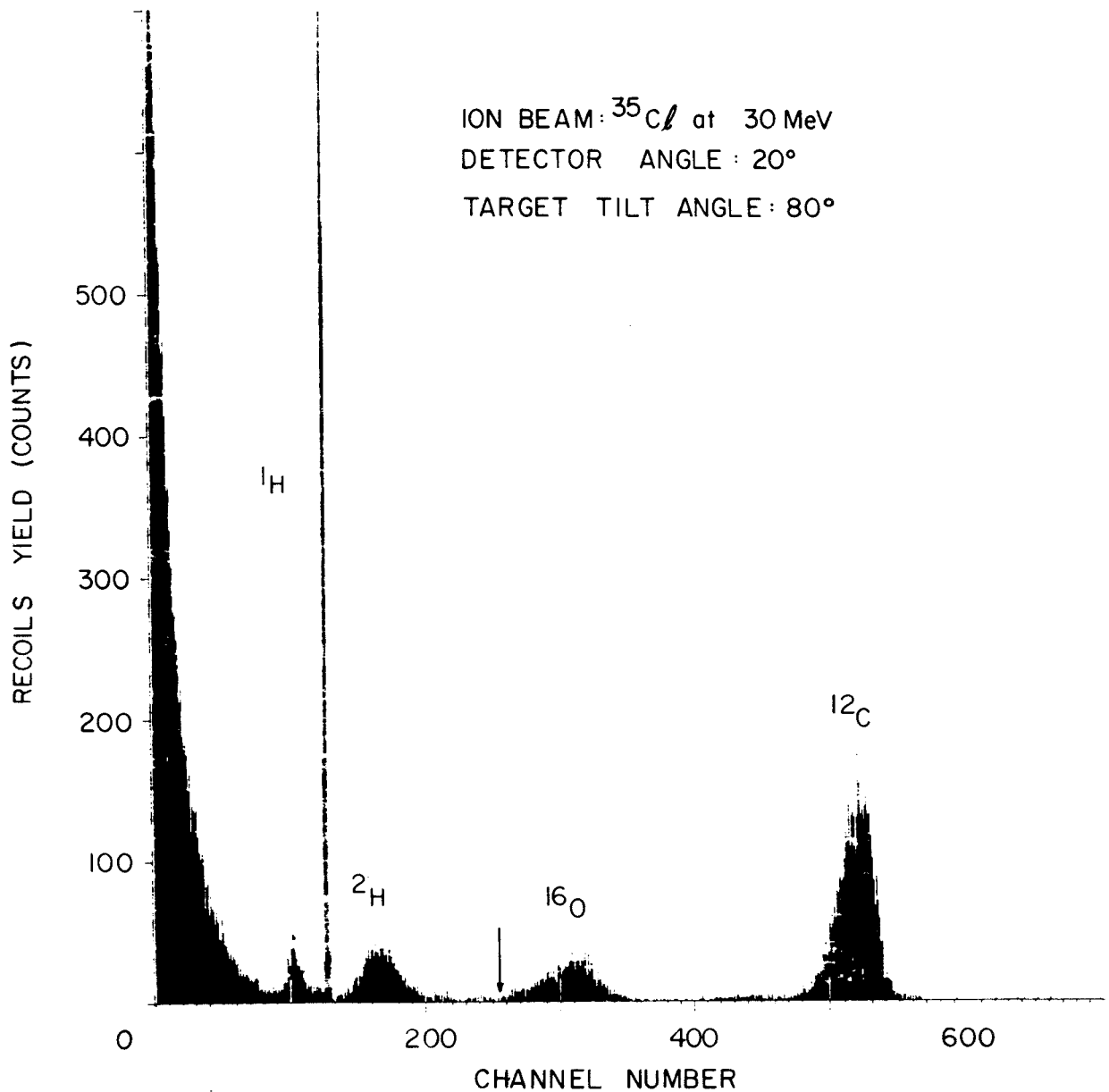


Figure 17. Spectrum of recoils in the detector. The sample was Si implanted with D. The arrow indicates the position of deuterium coming from the sample surface, calculated from the scattering kinematics and the energy loss in the mylar foil over the detector. Also shown is a large  $^1\text{H}$  peak presumably from hydrocarbons or water vapor on the sample's surface. The small  $^1\text{H}$  peak ( $\sim 10^{15}/\text{cm}^2$ ) may have come from the Si implantation which was originally made to create an amorphous layer on the Si samples prior to the H implantation.

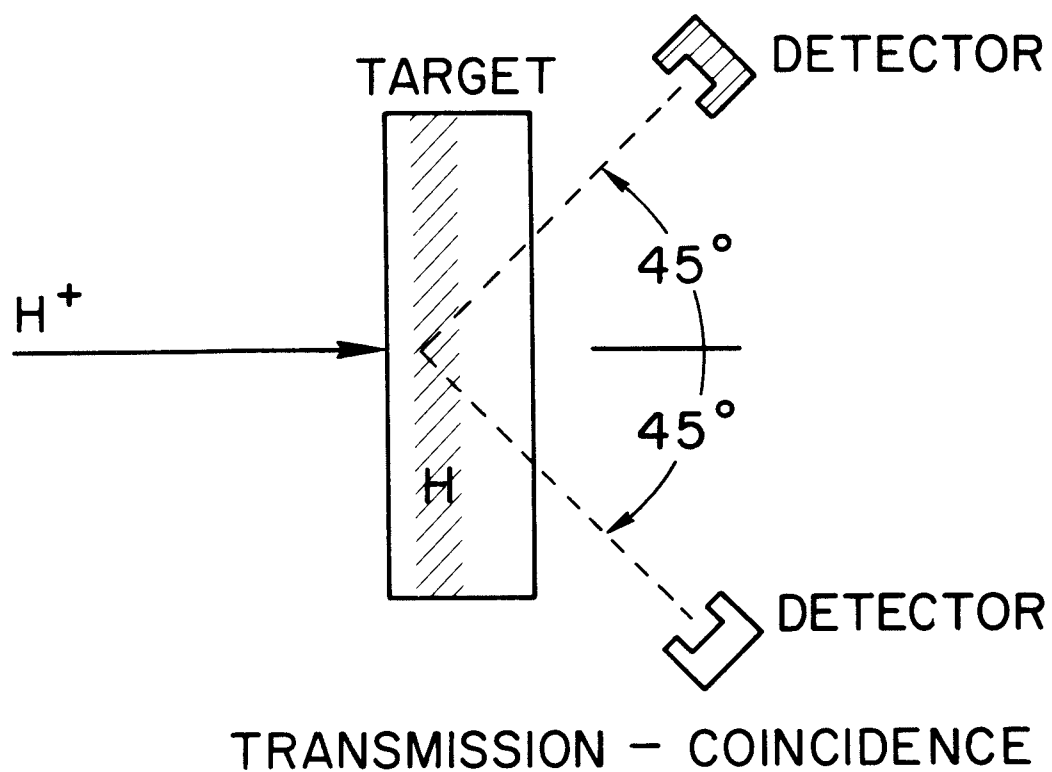


Figure 18. Experimental setup for the detection of H in thin materials using p-p (or d-d) coincidence for profiling hydrogen. The incident proton energy is chosen so that it will lose about 15% of its energy in the target. The sum of the energies of both protons detected in coincidence is used in the final spectrum.

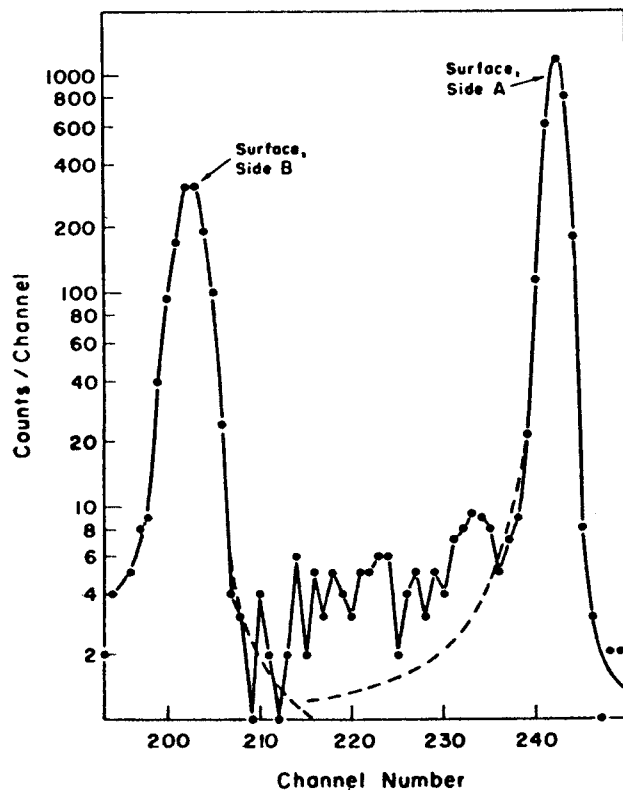


Figure 19. Experimental data results from a 125  $\mu\text{m}$  thick Al foil. Peaks are due to about 0.3  $\mu\text{g}/\text{cm}^2$  of H on the two surfaces, and the central portion is due to 0.7 ppm (weight) of H inside the foil. The decreased intensity and increased width of the left peak is due to multiple scattering.

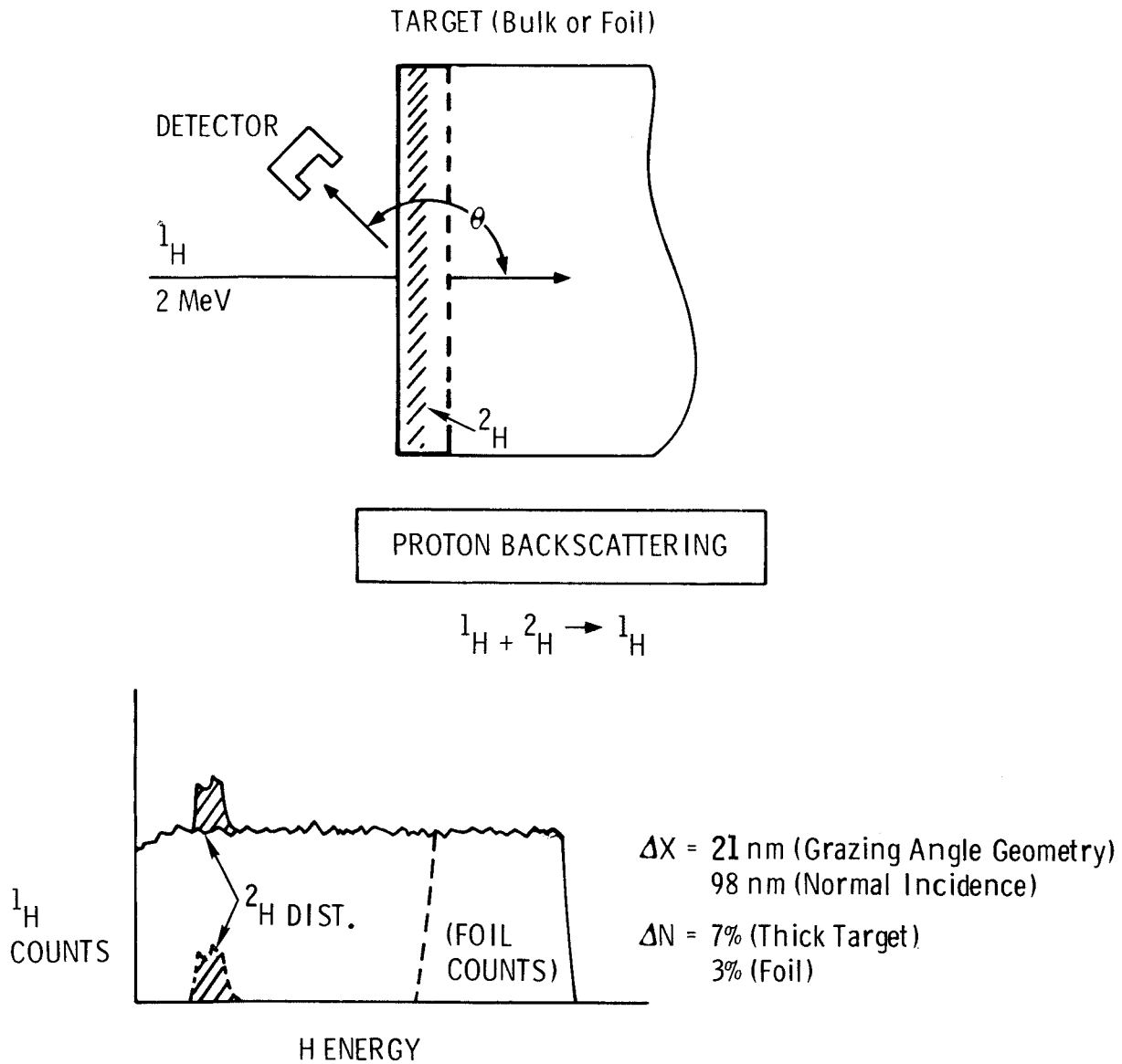


Figure 20. Schematic representation of the proton backscattering technique, Ref. 10. Both thick and foil targets can be used, with very low background when the latter is used. The upper part of this figure illustrates typical experimental geometry. The lower part illustrates typical data, with the continuous background coming from a thick target, and a cut-off of this occurring for a foil target. The  $\Delta X$  is typical depth resolution for Si for a normally incident beam, and the  $\Delta N$  is typical concentration sensitivity.

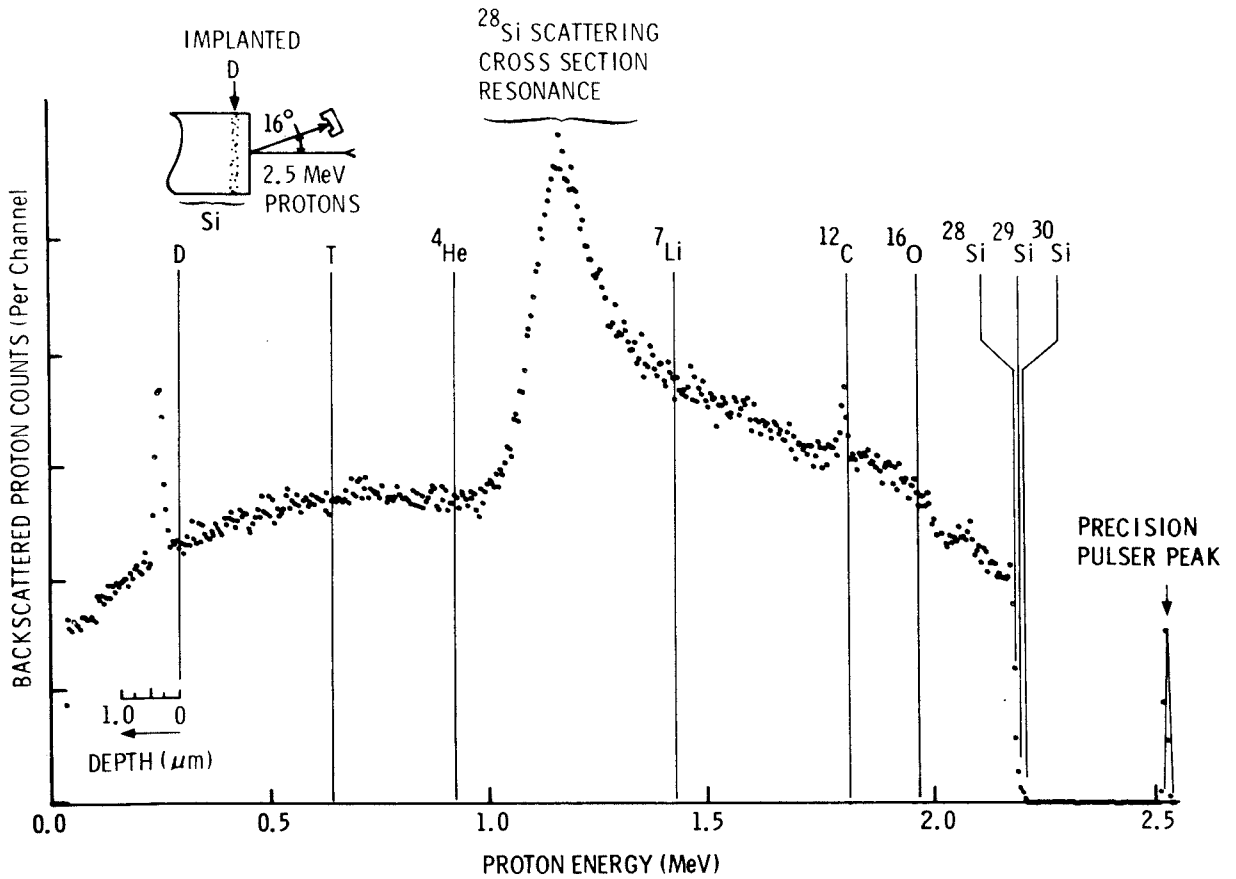


Figure 21. Representative backscattering spectrum of deuterium implanted silicon (31 keV,  $5 \times 10^{17}$  D/cm<sup>2</sup>). The deuterium peak is clearly visible at  $\approx 300$  keV. The surface position of other low atomic number elements is also indicated (note the surface carbon peak).

## ROUND-ROBIN 40keV PROTON IMPLANT

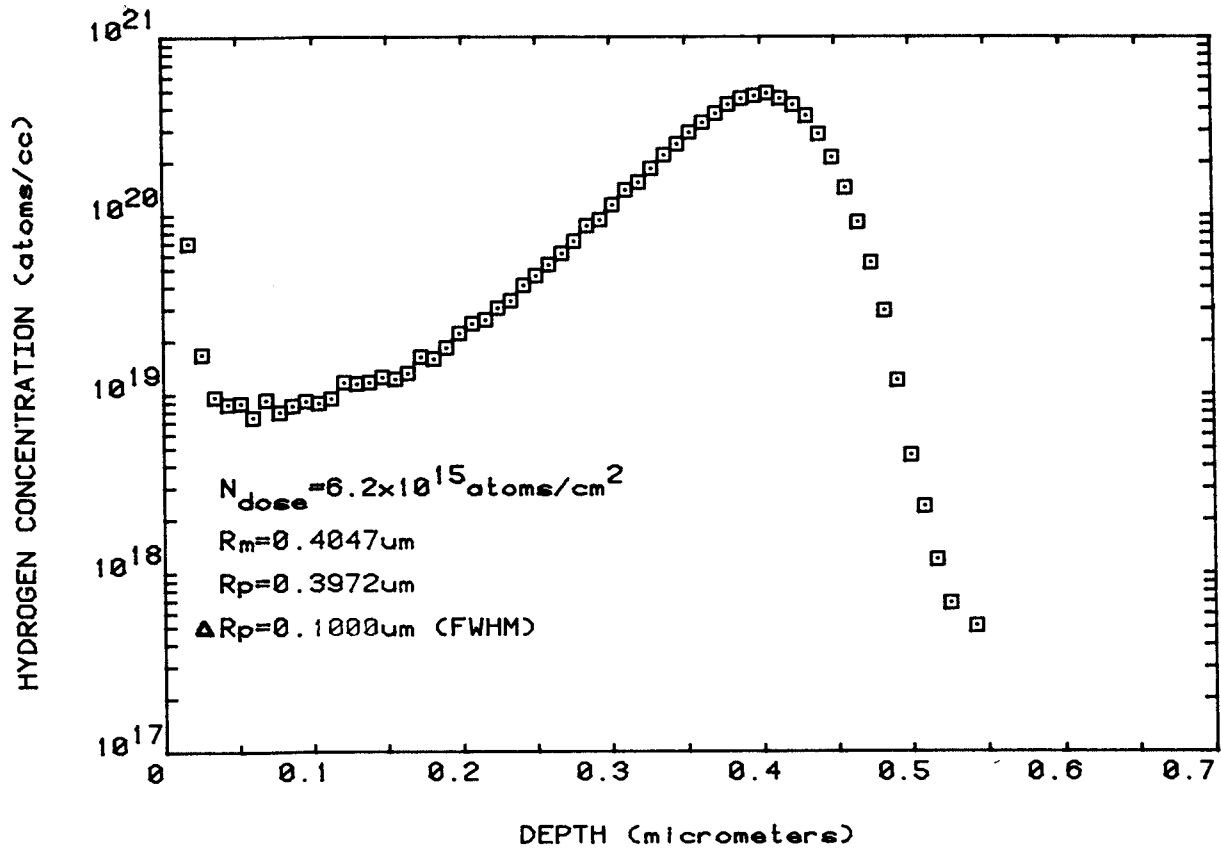


Figure 22. Typical SIMS data on the round-robin sample of protons in Si. The sputter beam was  $\text{Ar}^+$  at 11 keV (for details see Ref. 35).

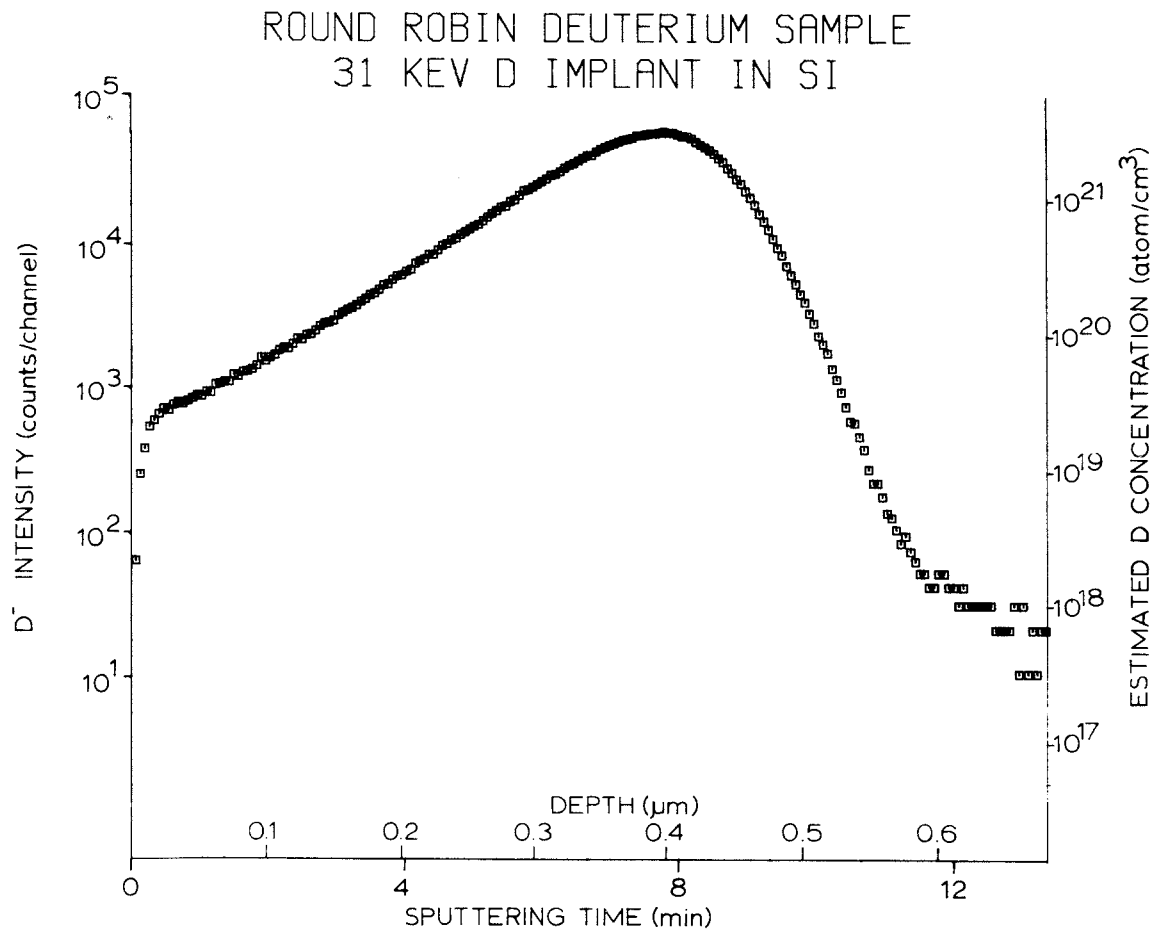


Figure 23. Typical SIMS data on the round-robin sample of deuterons in Si. The sputter beam was Cs<sup>+</sup> (for details see Ref. 36).

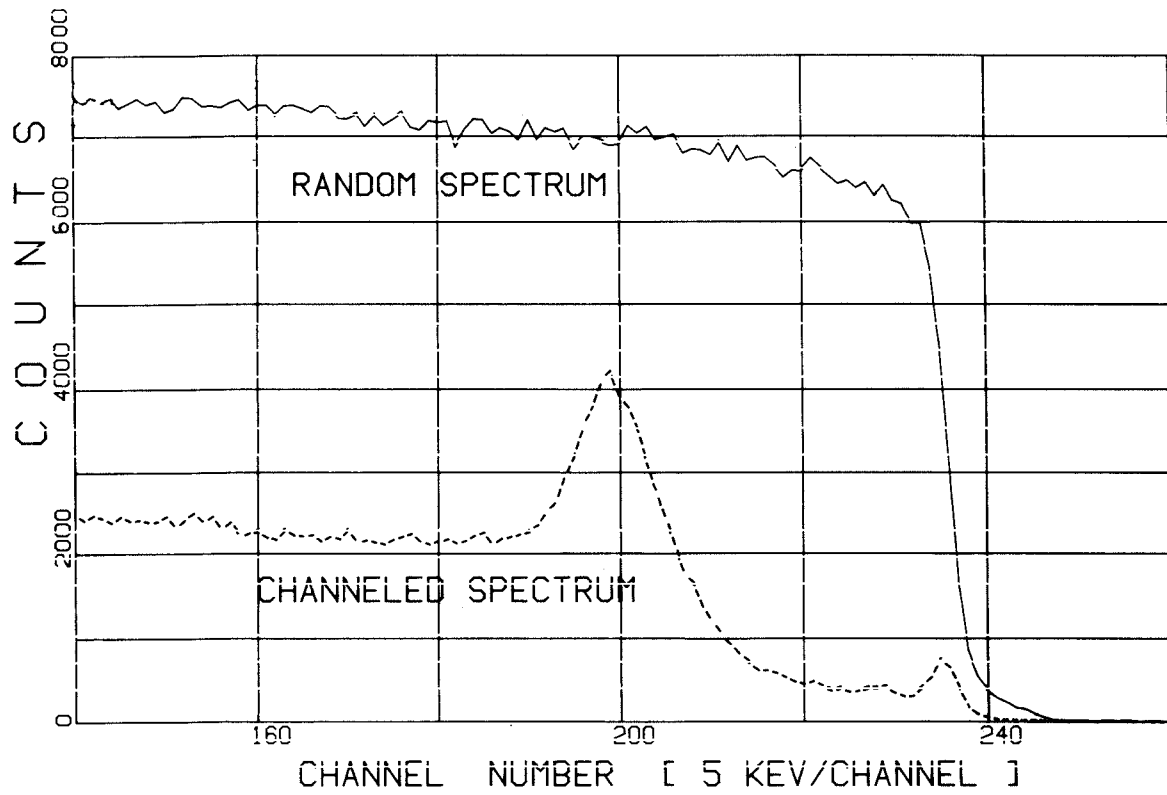


Figure 24. Random and channeled spectra of 2.1 MeV Helium ions backscattered from Si crystal damaged by hydrogen ion implantation.

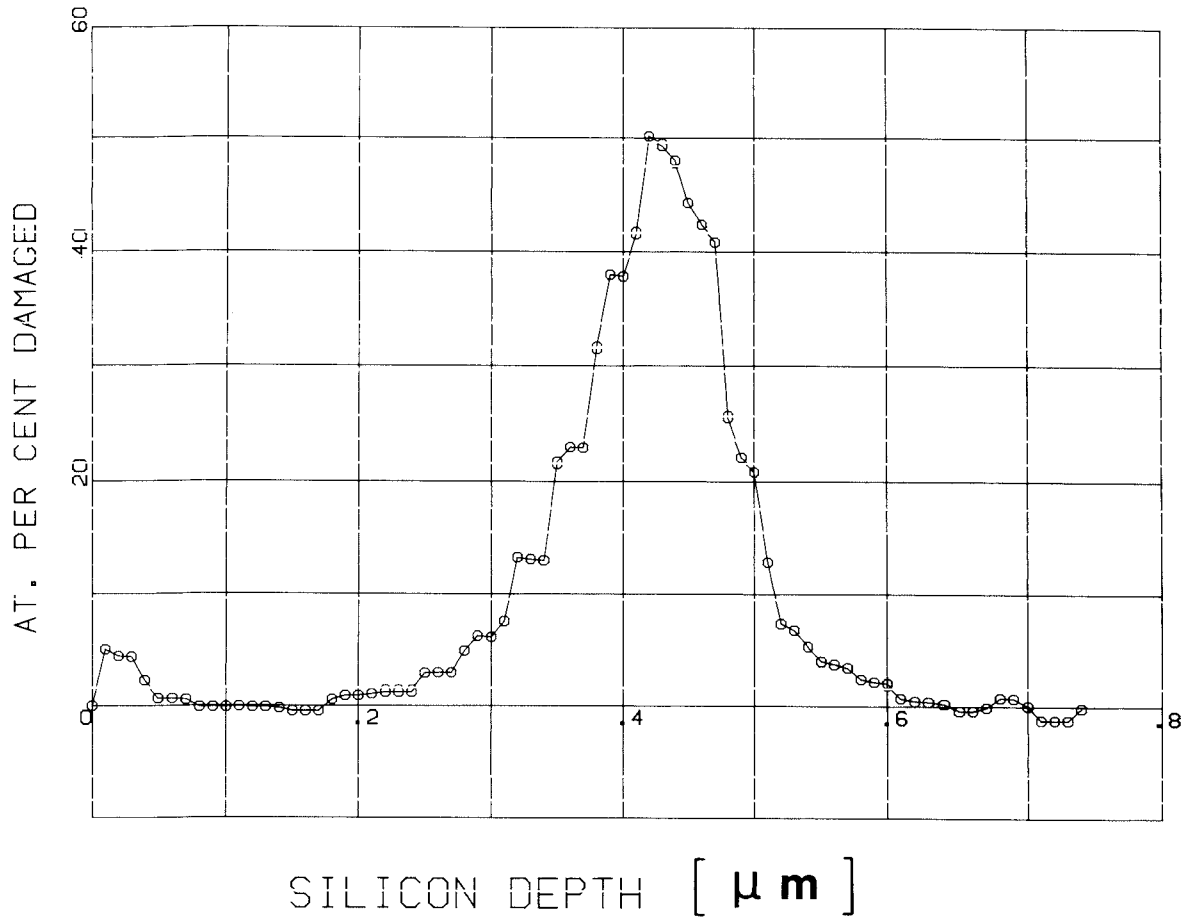


Figure 25. Damage distribution extracted from the channeling spectrum given in the previous figure.